Polymer Gels as Functional Soft Solids

By

Fut (Kuo) Yang

A thesis

presented to the University of Waterloo

in fulfillment of the

thesis requirement for the degree of

Doctor of Philosophy

in

Chemical Engineering

Waterloo, Ontario, Canada, 2020

Examining Committee Membership

The following served on the Examining Committee for this thesis. The decision of the Examining Committee is by majority vote.

External Examiner	Prof. Jin Zhang
	Chemical and Biochemical Engineering, Western University
Supervisor(s)	Prof. Boxin Zhao
	Chemical Engineering, University of Waterloo
Internal Member	Prof. Michael Pope
	Chemical Engineering, University of Waterloo
Internal Member	Prof. Christine Moresoli
	Chemical Engineering, University of Waterloo
Internal-external Member	Prof. Juewen Liu
	Chemistry, University of Waterloo

Author's Declaration

This thesis consists of material all of which I authored or co-authored: see Statement of Contributions included in the thesis. This is a true copy of the thesis, including any required final revisions, as accepted by my examiners.

I understand that my thesis may be made electronically available to the public.

Statement of Contributions

The research work described in Chapter 2 is prepared for publication, and is co-authored by myself, my supervisor, Dr. Boxin Zhao, my colleagues, Dr. Aleksander Cholewinski, and my collaborators, Dr. John Honek, Dr. Wei Wei, Dr. Michael Pope, Amanda Xu, Dr. Wei Zhang with the following contributions so far: F.Y. and B.Z. conceived the idea; F.Y. and A.C. designed all and performed almost all experiments; J.H. performed computer simulations; A.X. performed AFM measurements; M.P. provided critical feedback to the QCM results; W.W. provided discussion and inputs to mussel chemistry; W.Z. assisted with the tensile measurements; F.Y., A.C. and B.Z. analyzed and interpreted the results and wrote the manuscript; all authors helped shape the research, analysis and manuscript.

The research work described in Chapter 3 has been published and was co-authored by myself, my supervisor, Dr. Boxin Zhao, and my colleagues, Dr. Aleksander Cholewinski, Dr. Li Yu, and Dr. Geoffrey Rivers. with the following contribution: F.Y. conceived the idea and refined it with the help of A.C.; F.Y. and A.C. designed and performed the experiments; F.Y., A.C. and B.Z. analyzed and interpreted the results; F.Y., A.C. and B.Z. wrote the manuscript; L.Y. provided consultation and critical feedback to the manuscript; G.R. performed early mechanical measurements and additive manufacturing; B.Z. supervised and directed the research; all authors helped shape the research, analysis and manuscript.

Abstract

Polymer gels are polymer networks suspended in a liquid where chemical or physical crosslinks of the network maintain the physical form of the gels. They are a hybrid material that is between a liquid and a solid, making them unique among other solid matter. Gels are a common part of our lives with examples ranging from contact lens we use, noodles that we eat, to our very own biological tissues. Despite their ubiquitous nature, these materials have only recently been viewed as soft solids suitable for load-bearing applications due to advances in gel mechanics. While gels are generally fragile due to their low solid content, these advances demonstrated that through proper designs of the polymer network, one can impart gels with desirable properties such as high toughness, high stretchability, and self-healing, all without increasing the solid content. These properties allow the mechanical performance of gels to approach or even exceed that of pure solid materials. Consequently, gels have become a suitable and promising soft material candidate for rapidly growing fields in soft robotics and electronics, adhesion and adhesives, and biomedical engineering. To accommodate their increasingly sophisticated applications, these fields demand their materials to be highly functional, with material capabilities including actuation, stimuli-responsiveness, and shape memory effect. As a result, the aim of this thesis is to further explore polymer gels as functional soft solids by intersecting the design of gels with known scientific phenomena or principles to generate useful new properties.

First, we exploited the noncovalent interactions in gels and apply the concept of molecular recognition, commonly found in biological systems, to make a universal mussel-inspired nanoscale coating (polydopamine) into a "molecular double-sided tape" for the bonding and assembly of hydrogels (calcium-alginate, polyacrylamide, and polyvinyl alcohol) *via* non-covalent interactions. By incorporating and subsequently removing noncovalently interacting molecules that share the molecular characteristics of the hydrogels during coating formation, we imparted molecular conformations to the coating that are affinitive to the hydrogels. These conformational changes significantly enhanced (by about 2-3 folds) the

interfacial adhesion between the coating and hydrogels, allowing one to adhere hydrogels to different material surfaces with bonding strengths up to two orders of magnitude higher than if the bonding was performed directly on the bare surfaces without the coating. From a scientific perspective, this result illustrates that molecular recognition can be extended to recognize macroscopic materials beyond specific microscopic molecular structures. Additionally, it confirms the effect of molecular conformation on adhesion, which has historically baffled adhesion science. From a technical perspective, we designed experiments to further explore its potential practical applications. We demonstrated that by using a tougher hydrogel and following the bonding mechanics of mussel byssus, we could incorporate energy dissipation to further leverage the enhanced interfacial adhesion, showing that our approach can be useful in biomedical applications such as for the joining of artificial tendons.

Second, we leveraged the properties of liquid in gels and employed the phenomena of supercooling to resolve the engineering paradox of achieving both shape adaptability and load-bearing capability in materials science. A liquid can supercool and remain fluid below its freezing point due to the high energy barrier associated with the formation of "ice" crystals. This barrier effectively gives the liquid a metastable supercooled liquid state and a stable crystalline solid state that can be reversibly switched. By converting a supercooled liquid (melted sodium acetate trihydrate) into a gel by forming a polymer network (polyacrylic acid) in the liquid, the resulting gel has two stable and reversible solid states, making it one of the first solid materials with such behaviors. With the associated change in fluidity/rigidity of the liquid and the close molecular integration between the liquid and the polymer, the resulting gel attained a change in stiffness up to 10^4 times between the two states under the same environmental conditions, making the gel desirable for advanced applications. To this end, we have designed and performed experiments to demonstrate the potential of this material for applications including mechanical energy storage, stimuli-responsive smart construct, solid adhesive, shape memory material, and 3D printing.

Acknowledgements

Table of Contents

Chapter 1. Introduction and literature review

1.1 Overview of gels

Polymer gels are polymer networks suspended in a liquid where chemical (covalent) or physical (noncovalent) crosslinks in the network hold the physical form of the gels[1,2]. The typical mesh size of these polymer networks is approximately 10 nm[3]. Therefore, gels are hybrid materials rather than traditional composites since the molecular interactions and behaviors of their constituents are intertwined and indistinguishable from each other under this scale. Consequently, gels can be viewed as a material that is between solid and liquid, making them a distinctive class of materials among solid matter. As materials, gels are generally soft and wet, typically with an elastic modulus on the order of 10-100 kPa and a liquid content of more than 2/3 by weight, respectively[2]. They are commonly classified based on the type of liquid they contain (*e.g.* hydrogels for gels containing water and organogel for gels containing organic solvent) or the nature of their crosslinks (*e.g.* physical or chemical gels). The most common types of synthetic gels are water-based hydrogels, owing to their tissue-like properties and biocompatibilty[4].

The concept of gels can be traced as far back as the 19th century when the term 'gel' was clipped from the word 'gelatin' by the Scottish chemist Thomas Graham[5]. Nowadays, these materials directly and indirectly permeate our daily life from synthetic commercial products (*e.g.* contact lens) to natural biological materials (*e.g.* mammalian tissues). However, despite both their long history and prevalence, gels are still far from being applied to their full potential, especially considering their unique material properties. This is mainly due to their low solid content, which makes most gels fragile, with a fracture energy in the range of 0.1 to 1 J m^{-2} as found in jelly and tofu[6]. As a result, these materials have largely been viewed as an immobilized form of liquid rather than a solid material and the traditional applications of gels have mostly been limited to applications such as drug delivery and wound dressing that are not load-bearing. This perception of gels being weak has only recently (in the last decade or so) started to shift because of the advances in gel mechanics.

1.2 Gels as a load-bearing soft material

The work that pioneered a change in perception of gels involved the formation of a double network structure that consists of one rigid and one soft chemically crosslinked polymer networks that interpenetrate each other[7]. It was demonstrated that the resulting gel with only 10 wt.% of solid content can attain a fracture energy in the range of 100 to 1000 J m^{-2}, which is comparable to the toughness of cartilage and natural rubbers. The underlying mechanism is similar to that of bullet-proof glass, where the combination of soft and rigid counterparts helps distribute stresses, dissipate energy, and thus resist the formation and propagation of cracks that cause fracture. More recent important works involve the use of physical crosslinks that are reversible. For instance, when the secondary network was formed by crosslinking alginate polymers with calcium ions, the resulting gel not only was an order of magnitude tougher than the previous double network gel, with a fracture energy of more than 9,000 J m^{-2} at 10 wt.% of solid content, but was also highly stretchable, where the gel could be stretched more than 20 times its initial length[8]. This is owing to the ability of the ionic crosslinks in the secondary network to constantly reform after breaking; this reformation dissipates energy and keeps the gel's integrity during stretching. In another work, physical crosslinks for a single polymer network gel were formed *via* the complexation between catechol functionalities and ferric ions. As the ionic bonds associated with the complexation are among the strongest of physical bonds, the resulting gel could autonomously self-heal yet maintain near-covalent elastic moduli, which is unusual for self-healing materials[9].

The above-mentioned recent research efforts demonstrate that gels are far more broadly applicable than previously thought; without requiring much solid content, they can approach or even exceed the mechanical performance of pure solids. Thus, gels might be viewed as solids at the macroscopic scales but with liquid properties at the nanoscopic or molecular scales. They are suitable for applications requiring mechanical strength in areas such as soft robotics and electronics, adhesion and adhesives, and biomedical engineering. In the face of today's ever-growing demand for miniaturization and increasing

performance density, these areas increasingly demand soft materials that are ever more functional (*i.e.* having the right material properties such as stimuli-responsiveness, actuation, and shape memory effect for performing specific tasks). For instance, for effective medical treatment, one might want a soft material in a small package that can be remotely controlled and locally powered to move inside the body, release drugs, and disintegrate in a controlled manner in response to the right environmental cues. Accordingly, the aim of this work is to further explore strategies to impart gels with new and desirable functional properties meeting the rising demand.

1.3 Fundamental considerations in the design of functional gels

To design and engineer gels, one needs to consider and understand three key aspects that affect the behaviors of gels at different length scales. One aspect is that the intermolecular interactions in gels tend to be weaker and more selective than those in pure solids due to the screening effect of liquid[10]. In general, intermolecular interactions are the result of a balance between the attractions caused by noncovalent bonds between molecules and the separations caused by the repulsion and thermal fluctuations of these molecules. The above noncovalent bonds mainly include van der Waals attractions, hydrogen bonds, and ionic interactions. Among these, van der Waals attractions, consisting of dipole-dipole, dipole-induced dipole, and London dispersion forces, are ubiquitous. Expressions for the interactive energies of these bonds have been formulated for all but hydrogen bonds, revealing that all depend inversely on the dielectric constant of the medium in which they occur. For example, if we consider the liquid contained in gels as a medium and take water as the example liquid, Coulomb's Law indicates that electrostatic interactions in gels are at least 80 times weaker than in pure solids, given that the dielectric constants for water and vacuum at 25°C are 80 and 1, respectively. Liquids other than water, depending on the polarity of their molecules, are expected to have a similar effect. Additionally, as these noncovalent bonds must also compete with the bonds formed by liquid, they occur much more selectively. For instance, noncovalent interactions that are stable in vacuum tend to dissociate in liquid due to the associated changes in free energy. This resulting selectivity drives the organization of molecules in gels *via* phenomena such as hydrophobic interactions and electrical double layers.

Another aspect is that the behaviors of the polymer network and the liquid are heavily entangled with one another. When the liquid is a good solvent to the polymer network, liquid molecules can permeate into the free volume between the polymer chains of the network, increasing the chains' mobility[11–13]. This is because the liquid can reduce the adhesion between the polymer chains by screening their intermolecular interactions, increasing their intermolecular distance, and acting as a lubricant. This is the

reason why many polymers that are typically rigid in air become soft when they are solvated. On the other hand, liquid molecules in the vicinity (normally on the order of nanometers) of the chains become less mobile than liquid molecules in the bulk, showing two states depending on their interactions with the polymer chains. For one state, when the interactions between the polymer and liquid are stronger than that of the liquid itself (*e.g.* between hydrophilic polymer segments and water), the liquid molecules are bound to the polymer chains with non-random average orientation. As it takes more energy to remove them from the chains, these molecules behave differently than the ones from the bulk and they tend to be harder to freeze and evaporate[11,14]. For the other state, when the interactions between the polymer and the liquid are weaker than that of the liquid itself (*e.g.* between hydrophobic polymer segments and water), the liquid molecules are organized around the polymer chains to maximize their interactions with the liquid molecules in the bulk. These interactions result in a cage-like structure for these liquid molecules near the polymer, for which the structure is reminiscent to that of surface tension due to the lack of interactions between the liquid and the polymer[15]. As this structure is entropically unfavorable, there is a tendency for the contact between the liquid and the polymer to minimize, leading to phenomena such as the hydrophobic effect, which can cause the polymer chains to fold, aggregate, and phase separate from the liquid. These entangled interactions between polymer chains and liquid molecules dictate many microscopic behaviors of gels. These behaviors include the molecular conformation of the polymer chains, where the segments of the polymer chains would extend or contract depending on the strength of their interactions with the liquid and their inherent elasticity associated with the angles and rotations of their covalent bonds[16]. Conversely, these interactions with the polymer chains would also cause confinement of the liquid. As the length scale of this confinement approaches the length scale of the molecular interactions and the position correlation of the liquid, the liquid would have a greater structural order and a longer relaxation time (*i.e.* the time in which the liquid structure remains unchanged and solid-like)[17,18].

This confinement often leads to multiple phases of the liquid in gels at the microscopic level, with varying heat and mass transfer properties, viscosities, and densities for each phase.

The last aspect is that the overall miscibility between the polymer network and the liquid is largely determined by enthalpy. According to the Flory-Huggins solution theory, the contribution of entropy (ΔS_{mix}) to the free energy of mixing (ΔG_{mix}) for a polymer network in liquid is significantly smaller than that between small molecules and liquid. This is because the linkages or size of the polymer network imposes restrictions on the possible mixing configurations (microstates)[12]. Consequently, the free energy of mixing is mostly enthalpic (ΔH_{mix}), depending on the overall change in heat for the molecular interactions associated with the assembly of polymer-liquid and the disassembly of liquid-liquid and polymer-polymer. This change might be quantified by the Flory-Huggins interaction parameter (χ), which can be estimated through solubility parameters such as Hildebrand or Hansen on the basis of "like dissolves like"[19]. For the polymers and the liquid to be miscible with each other, the interaction parameter should be negative or a slightly positive number (normally less than 0.5), corresponding to the mixing process being exothermic or slightly endothermic, respectively. The miscibility between the polymer network and the liquid contributes strongly to the macroscopic behaviors of gels. First, it defines the density and homogeneity of the polymer network, as the swelling of the network is a balance between the solvating forces and the elastic retractive forces of the polymer chains[12]. The resulting state of the polymer network in turn affects the gels' macroscopic properties, including mass transport and mechanical response. Second, the miscibility also affects the liquid retention of gels[1]. For partially miscible gels (*e.g.* tofu), the osmotic pressure is relatively small since the amount of solvated component is small. This leads to poor liquid retention, where the liquid in gels is easily squeezed out under compression. This contrasts with miscible gels (*e.g.* jelly), where the gel would rather break under compression than release its liquid.

1.4 Synthesis, design, and characterization of functional gels

In terms of material synthesis and design, gels are typically formed by *in-situ* crosslinking of polymers in the liquid where the polymers are at least partially miscible with the liquid. The choices for the constituents are wide ranged. The network may be formed from polymers that are homopolymeric or copolymeric, natural or synthetic, hydrophilic or hydrophobic, ionic or nonionic, and polymerized before or during gelation, while the liquid may consist of aqueous solutions, ionic liquids, organic solvents, and non-aqueous inorganic solvents. By selecting the right formulation, one can create gels with functional properties suitable for different applications. Here, we highlight some key examples, with the first few examples focusing on the engineering of the polymer network and the last few focusing on the engineering of the liquid in gels. One classic example is that one can make gels stimuli-responsive by incorporating polymers or polymeric components such as polyelectrolyte and poly(N-isopropylacrylamide) that change their chemical potential in the presence of stimuli such as pH, heat, or light[20]. This change in chemical potential would cause a shift in the interactions between the polymer network and the liquid. Consequently, this shift would make the polymer network swell or shrink, resulting in a significant change in the gel's volume. As a result, these gels are useful for sensing, smart release of drugs, and actuation. Another example is that one can impart gels with complex material behaviors by engineering the connectivity of the gels' network, including the use of multiple polymer networks, reversible crosslinks, and supramolecular coupling, leading to properties such as toughness[6], self-healing[21], stretchability[22], or even on-demand sol-gel transitions[23]. As another example, one can turn gels into underwater adhesives based on noncovalent bonds by incorporating catechol and other synergistic functional groups into the polymer network[24]. These gels are not just useful as adhesives for surgeries and tissue engineering but have important implications for the joining of these gels with other materials, which is needed for many practical applications (*e.g.* being part of a device). For engineering the liquid, one example would be using electrolyte as the liquid component of the gel, allowing electrical signals to be transmitted through the

mobilization of ions in the liquid[3]. These gels are useful as soft conductors for applications such as wearable electronics and artificial axons. The final example exploits the presence of liquid on the surface of gels; one can make gels' surface slippery by incorporating liquids with extremely low surface energies[25]. These gels are useful for applications involving anti-fouling, anti-adhesion of bacteria, anti-icing, and low friction.

To characterize these functional properties, common techniques include: swelling measurements, which compare the dry and wet weight or volume of gels; indentation measurements, where the work of adhesion and the elasticity of a gel can be extracted from indenting the gel with another material using contact mechanics such as the JRK theory; contact angle measurements, where the surface energy and the wetting characteristics of a gel's surface can be quantified by examining the contact behaviors of different liquids against the gel's surface; mechanical measurements, including tensile, compression, and rheological tests, where the gel's mechanical response (including the elastic, viscous, and plastic contributions to the response) can be obtained by examining the force and displacement of gels under deformation; adhesion measurements including tensile pull-off, lap-shear, peeling, and friction tests, where the bonding strength between a gel and another material can be attained by measuring the corresponding force of separation; and thermal measurements, including thermogravimetric analysis and differential scanning calorimetry, where the characteristics and confinement of the liquid in gels can be determined by examining the changes in weight or heat absorption of a gel with respect to different temperature profiles.

1.5 Thesis outlines, research problems and objectives

With gels showing potential to be functional soft solids, the overall objective of this thesis is to combine the design of gels with known scientific phenomena or principles, to generate new useful capabilities that can address fundamental and ongoing challenges in materials science. Additionally, we explore both the fundamental and practical aspects of these engineered gels. The thesis begins with this introductory section, Chapter 1, that covers background information and relevant literature. This is followed by two research chapters presented in the format of research articles. The contents in Chapter 2 focus are almost ready for submission, while Chapter 3 has been published. Finally, an overall conclusion and recommendations for future work are presented in Chapter 4. Each research chapter has its own introduction, results and discussion, conclusion, and supplemental information.

One major challenge in materials science is wet adhesion, like in the case of bonding hydrogels, which is important for many biomedical applications. Due to the screening effect of liquid, noncovalent interactions are generally weaker by orders of magnitude in wet than in dry conditions, rendering adhesion almost nonexistent in the absence of covalent bonding. Consequently, almost all existing approaches for the bonding of hydrogels rely on forming covalent bonds at the interface. However, compared to covalent interactions, noncovalent interactions should lead to a more universal solution for bonding. Inspired by the adhesion of molecules in biological systems, in Chapter 2 of this thesis, we explored the bonding of hydrogels with noncovalent interactions by applying the idea of molecular recognition to gels. Molecular recognition is a fundamental principle behind the interactions of proteins and biomolecules and is the basis for the concept of "lock and key", where matching molecular conformations leads to adhesion. While this has conventionally been limited to binding of small molecules or proteins to a surface, we hypothesized in this work that molecular recognition can also be applicable to macroscopic adhesion. To test this hypothesis, we selected a mussel-inspired hydrogel coating, polydopamine, as a platform for its ability to establish a range of noncovalent interactions similar to

proteins in water and for its ability to coat virtually to all material surfaces. We tested the bonding of three common hydrogel systems (calcium-alginate, polyacrylamide, and polyvinyl alcohol) to the coating. To enhance the molecular recognition (noncovalent adhesion) of the coating to one of the hydrogels, we incorporated and subsequently removed noncovalently interacting guest molecules that shared similarities to the particular hydrogel during the formation of polydopamine to modify its molecular conformation. We found that when the hydrogel was subsequently formed in-situ on the coating, the interfacial adhesion between the hydrogels and coating was substantially higher (2-3 folds) across different length scales (ranging from molecular to macroscopic) than it was without conformational changes. Consequently, this increase in adhesion effectively turned polydopamine into a molecular double-sided tape for hydrogels, allowing one to bond hydrogels to different materials with the use of the coating, especially when coupled with proper energy dissipation. Overall, these results also confirm the role of molecular conformation in interfacial adhesion, which has been speculated since close to the inception of adhesion science.

Another major challenge in materials science is the paradox between achieving both shape-adaptability and load-bearing capability. While many materials may overcome this paradox by changing their stiffness upon exposure to stimuli (*e.g.* heat), they require a change in the environment (*e.g.* a different environmental temperature) to maintain their stiffness change. This requirement of environmental change poses significant restrictions on the application of these materials. To overcome this issue, one would need the material to be a two-in-one solid, having two stable and reversible solid states, so that the material can have different stiffnesses under the exact same environmental conditions. Existing approaches for creating two-in-one solids rely on chemical or mechanical metastability. In Chapter 3 of this thesis, we created a two-in-one solid with physical metastability by taking the phenomenon of supercooling of liquids and applying it to gels. Liquids can supercool and remain fluid below their freezing point due to the high energy barrier associated with the formation of "ice" crystals. This barrier effectively

gives the liquid a metastable supercooled liquid state and a stable crystalline solid state that can be reversibly switched. One of the most well-known supercooled liquids is sodium acetate trihydrate. By forming crosslinked polyacrylic acid in sodium acetate trihydrate, we created a gel that has two reversible and stable solid states. As crystallization could immobilize all liquid molecules that account for the flexibility and softness of the gel, the resulting gel can attain a record-breaking change in stiffness among all solid materials, more than 10^4 times between its supercooled state and its crystallized state. This property makes the gel useful for soft robotics, adhesion and adhesives, and other advanced applications.

The last chapter provide conclusions of findings and recommendations for future research.

Chapter 2. Hydrogel Adhesion via Interfacial Conformation: Fundamentals and Applications

2.1 Summary

This chapter studied the connections between hydrogel adhesion and interfacial conformation. Since the inception of adhesion science more than five decades ago, adhesion at an interface has long been recognized as beyond two-dimensional. Similarly, molecular conformation – the three-dimensional arrangement of atoms in a molecule – is ubiquitous in biology and fundamental to the binding of biomolecules. However, the connection between these concepts, which could link molecular conformation in biology to micro- and macroscopic adhesion in materials science, remains elusive. Herein, we examined this connection by manipulating the molecular conformation of a mussel-inspired universal coating, imparting a memory for recognizing different hydrogels. We confirmed this could lead to a significant increase in interfacial adhesion between the coating and hydrogels (about several folds) across a broad range of length scales, from molecular to macroscopic. Furthermore, we demonstrated that imparting memory could be a general and facile approach for enhancing interfacial adhesion and with suitable energy dissipations, might be used for the bonding of materials.

2.2 Introduction

All proteins stick or bind to other molecules *via* numerous noncovalent interactions including van der Waals forces, hydrogen bonding, electrostatic, and hydrophobic interactions. As these interactions are nonspecific and individually weak, for a protein to recognize and bind to the desired ligand out of thousands of other molecules, many of these interactions must occur simultaneously. Proteins achieve this through molecular conformation (the arrangement of atoms in a molecule), where the geometric organization of the functional groups matches the reciprocal functionality of the ligand[26].

This principle behind molecular recognition – using conformation to create specificity out of nonspecific interactions – has inspired biotechnologies that include molecular imprinting for biosensors or chromatography. However, its use so far has been limited to localized adhesion – binding of proteins, specific supramolecular structures, and other molecules – to a surface. We suspect that we can extend molecular recognition to a more general and larger scale for micro/macroscopic adhesion between surfaces and hypothesized that we can impart a "memory" to a surface for a material by manipulating its molecular conformation, enhancing their interfacial adhesion. This connection between interfacial conformation and adhesion, to the best of our knowledge, has not been confirmed, though it has long been speculated in adhesion science since the 1970s[27], where the concept of the three-dimensional adhesive interface (*i.e.* adhesive interphase) was introduced[28,29].

To verify our hypothesis, we utilize a mussel-inspired universal coating, polydopamine, as a platform. Dopamine is a small biomolecule that is mimetic to mussel adhesive proteins due to its catechol and amine functionalities. In particular, the catechol functionality is capable of displacing water molecules and forming a range of noncovalent bonds similar to proteins with underwater surfaces[30,31], while the amine functionality has been shown to assist the catechol's binding[32]. Under aqueous alkaline conditions, dopamine self-polymerizes to form polydopamine, which can coat virtually any surfaces[33]. The exact mechanism is still not clear, but it is generally accepted that the formation process is dependent on both

noncovalent and covalent interactions[34–39]. By incorporating small, noncovalently-interacting guest molecules during its formation process, one can tune the molecular conformation of polydopamine, which has led to molecular imprinting of polydopamine for biosensing[40].

In this work, we employed guest molecules affinitive to specific hydrogels to enhance polydopamine's molecular recognition to these hydrogels and measured their adhesion to polydopamine in a fully hydrated environment (similar to that of proteins, with minimal interactions of ubiquitous van der Waals forces) at the molecular and micro/macroscopic levels. This work demonstrates that molecular recognition can be exploited as a general approach to enhance interfacial adhesion (

Fig. 2.1), confirming matching the molecular conformation of one surface for another could lead to a significant increase in interfacial adhesion. When leveraged with proper energy dissipation, it could be employed for bonding applications.
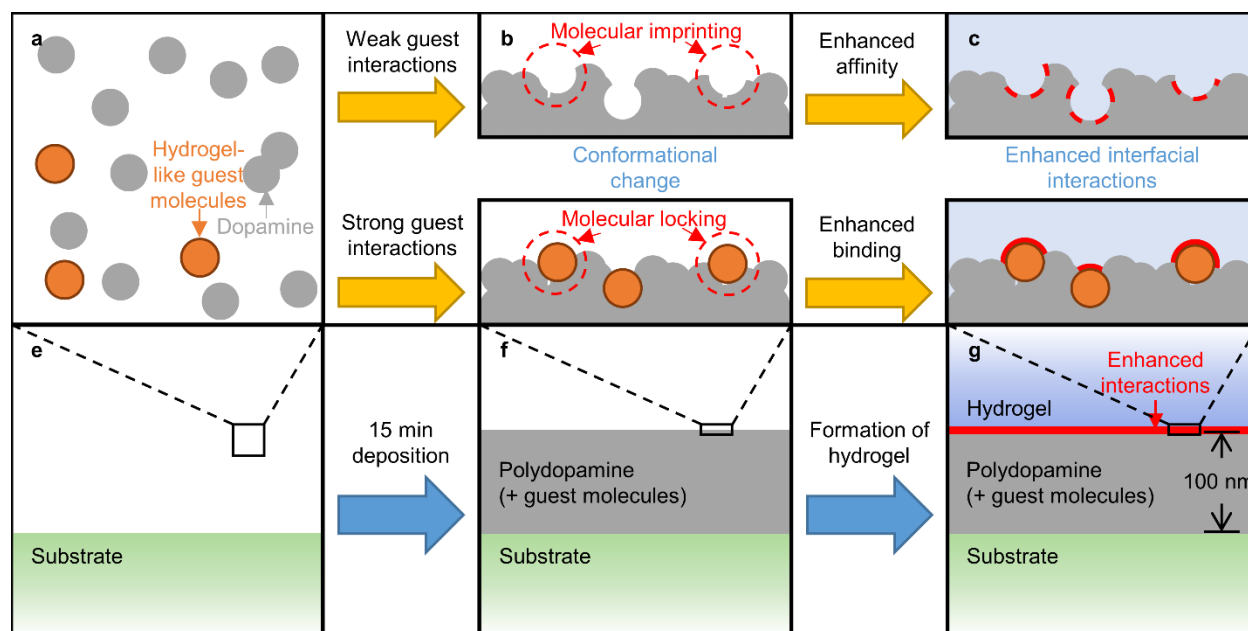
Fig. 2.1: Enhancing interfacial adhesion by imparting molecular memory. a-g, The process consists of first coating a substrate with polydopamine by immersing the substrate in a solution (**e**) consisting of dopamine molecules and a small amount of non-covalently interacting guest molecules affinitive to a hydrogel (**a**), then rinsing the coating to remove unbound molecules (**f**), and finally forming the hydrogel

in-situ on the coated substrate (**g**); when the interactions between the guests and the dopamine molecules are weak, guest molecules leave imprints on the polydopamine surface; in contrast, when the interactions are strong, guests are locked into polydopamine (**b**); in both cases, the associated conformational change in polydopamine results in enhanced adhesion to the hydrogel (**c**).

2.3 Methodology, materials and characterizations

Formation of polydopamine coating

Polydopamine coatings were formed on substrates using a modified version of the method employed by Lee and coworkers[33]. In short, a coating solution was prepared by mixing 2 mg/mL dopamine hydrochloride (Sigma-Aldrich), 0.2 mg/mL ammonium persulfate (≥98.0%; Sigma-Aldrich), and guest molecules in a solution containing 10 mM tris(hydroxymethyl)aminomethane (≥99.8%; Sigma-Aldrich) buffered at pH 8.5 with hydrochloric acid (37%; Sigma-Aldrich). Unless indicated otherwise, the guests were 0.2 mg/mL iron(III) nitrate nonahydrate (≥98%; Sigma-Aldrich) for the +Fe system, 0.2 mg/mL N,N'-methylenebis(acrylamide) (99%; Sigma-Aldrich) for the +MBAA system, 1 mg/mL 2,4-pentanediol (98%; Sigma-Aldrich) for the +diOH system, and 0.2 mg/mL iron(III) nitrate nonahydrate and 0.2 mg/mL N,N'-methylenebis(acrylamide) for the hybrid hydrogel system. After preparation, the substrates to be coated were immediately immersed in the coating solution for 15 minutes and then taken out and thoroughly rinsed with deionized water under ambient conditions.

Water content of polydopamine coating

The water content of polydopamine coating was measured by estimating the weight of polydopamine aggregates at 100% humidity and comparing with their fully dried weight. In short, polydopamine aggregates (which were self-assembled during the coating process) in coating solution were collected, washed with deionized water, and stored in an environmental chamber (BTL-433; ESPEC) at 25°C and 90% relative humidity until all excess water was evaporated and equilibrium was reached. The weight of the samples was then periodically measured and was recorded once it had stabilized with respect to the relative humidity at 90%, 80%, 70%, 60%, and 50%. Afterwards, these samples were fully dried in oven at 50°C to obtain the dry weight. The wet weight of polydopamine under fully hydrated conditions were obtained by extrapolating the weight to 100% relative humidity based on the data collected. The water

content of polydopamine was calculated by dividing the difference between the wet weight and dry weight by the wet weight.

Thickness of polydopamine coating

The thickness of polydopamine was estimated by coating glass microspheres (9-13 µm; Sigma-Aldrich) with polydopamine. The surface area of glass per mass of microspheres was determined by surface area analysis (Gemini VII Surface Area Analyzer; Micromeritics). The weight of the polydopamine coating on the microspheres per mass of microspheres was obtained using thermal gravimetric analysis (Q500 Thermogravimetric Analyzer; TA Instruments) by burning away the coating with oxygen. The areal density of polydopamine was then calculated by dividing the coating weight over the glass surface area. Assuming a density of water (which is typical for most polymers) and based on the measured water content, this areal density was converted into the dry and wet thickness of polydopamine.

Chemical characterization of polydopamine

The chemical characteristics of polydopamine were determined by performing Raman spectroscopy (MicroRaman; Renishaw) on polydopamine aggregates (which were collected from coating solutions, washed, and dried in air) with a 633 nm He-Ne laser source, Fourier-transform infrared spectroscopy (520; Nicolet) on polydopamine aggregates compressed with KBr, and x-ray photoelectron spectroscopy (ESCALab-250; Thermo Scientific) on polydopamine coatings coated on gold with a non-monochromatic Al Kα twin anode radiation source, a hemispherical analyzer (of 150 mm mean radius), and a working pressure of 5×10^{-10} mbar.

Physical characterization of polydopamine

The physical characteristics of polydopamine were determined by performing atomic force microscopy (Nanoscope MultiMode; Veeco) in tapping mode and water contact angle measurements using the sessile drop method with a custom MATLAB program to obtain the contact angles through an elliptical best-fit model, on polydopamine coatings coated on PDMS (10:1 mixing ratio, 90°C for 90 min; Sylgard 184).

Micro-indentation measurements on interfacial adhesion

The adhesion between polydopamine and gel solutions were measured by micro-indentation using a custom equipment setup. The setup included an inverted microscope (Axio Observer.Z1m; ZEISS) and side camera for viewing the system, as well as a force sensor and micromechanical stage for moving the probe and measuring force. The tests were carried out in a fully hydrated environment using a hemispherical PDMS probe (10:1 mixing ratio, 90°C for 90 min) and a glass slide, with the samples to be tested between the two surfaces. Both surfaces were coated with polydopamine and the gel, which varied based on which system was investigated, was spread on the probe, which was then brought into contact with the glass slide at a specific preload force for a period of time. For the +Fe system, the gel solution consisted of 5 wt.% sodium alginate (from brown algae, medium viscosity; Sigma-Aldrich) relative to water. The test was carried out in 0.1 M aqueous acetic acid (Glacial; Fisher Scientific), which is the condition used to dissolve calcium carbonate for crosslinking sodium alginate in tensile pull-off measurements, with a preload of 0.5 g. After reaching this force, the probe was held in position for 60 min to establish adhesive contact. For the +MBAA system, the gel solution consisted of 20 wt.% acrylamide (≥99%; Sigma-Aldrich), 3 wt.% polyacrylamide (nonionic water-soluble polymer; Sigma-Aldrich), and 1 wt.% initiator containing 10% v/v of 2,2-diethoxyacetophenone (>95%; Sigma-Aldrich) in dimethyl sulfoxide (BioReagents; Fisher Scientific) relative to the water. The test was carried out in deionized water with a preload of 1 g. After reaching this force, the system was exposed to ultraviolet light (X-Cite 120 Q; Excelitas Technologies) for 5 min, with 10 min waiting before and after light exposure to stabilize the sample temperature and establish adhesive contact. For the +diOH system, the gel solution consisted of 5 wt.% poly(vinyl alcohol) (Mw. 146,000-186,000; Sigma-Aldrich) relative to water. The test was carried out in deionized water with a preload of 3 g. After reaching this force, the probe was held in position for 30 min to establish adhesive contact. After the holding period for each system, the probe was retracted from the glass surface at a rate of 0.1 μm/s

until complete separation. Force and displacement values were recorded using a custom LabVIEW program.

Quartz crystal microbalance measurements on molecular affinity

The adsorption of solutes on polydopamine coatings under aqueous conditions were measured by quartz crystal microbalance (AWS A20; AWSensors), using polished Ti/Au quartz crystals (keyhole 14 mm, 9 MHz; AWSensors). In a typical test, the crystals were coated with polydopamine according to the coating procedures and afterwards, were loaded into a static chamber containing 5 mL of deionized water and stabilized at 25°C overnight. After stabilization, increasing amounts of solutes were manually added into aqueous solution contained in the chamber using a micropipette at different time points. For +MBAA, the solute was an aqueous solution of N,N'-methylenebis(acrylamide) at a concentration of 10 g/L. For +diOH, the solute was neat 2,4-pentanediol. The corresponding changes in the resonance frequency, Δf, and the energy dissipation, ΔD, of the polydopamine coated crystal were recorded. For reuse, the crystals were cleaned by exposing to UV-ozone (PSD Pro; Novascan) for more than 2 hours and rinsing with deionized water.

Monte Carlo simulations on binding energy

To simulate the binding interactions between polydopamine and polymers, amorphous cells of either polyacrylamide or polyvinyl alcohol were constructed at a cell density of 1 g/cm^3 based on the random entangled growth of 40 atactic polymer chains, where each chain contained 40 monomers. This involved the use of Maestro (Release 2019-4; Schrodinger, Inc.) and the Polymer Builder module to build the amorphous cells. Each cell was then fully solvated in water (SPC water; with boundary conditions, cubic buffer of 10Å; OPLS3e force field) and relaxed for 1000 ps utilizing Desmond (D. E. Shaw Research). Water molecules were then removed to allow the surfaces of the polymers to be exposed to the dopamine analogs and the Disordered System Builder was utilized to prepare a disordered molecular system containing 10 copies of the particular dopamine analog as the probe ensemble and one copy of the

19

particular polymer cell (set as a planar interface). The interface on each cell was localized to provide an interface with the best uniform surface possible, usually the "Best Fit to All Atoms", providing the required interface for subsequent studies. Additional options set for the Disorder System Builder were generally default options such as OPLS3e force field and Steric Pack. Once the disordered system was built, the Adsorption Site Finder module was employed with the following settings: maximum structures kept, 10; Minimize setting was employed; simulation temperatures, 900K/600K/300K with 3000 iterations at each temperature; and other settings were default settings and included restricting the search to the region near the polymer surface with a 5 Å dynamic region being employed. The binding energies (E) were computed both at the initial unoptimized positions and subsequently after optimization according to the equation:

$$E_{binding} = E_{substrate} + E_{adsorbate} - E_{substrate+adsorbate}$$ **S. Eq. 2.1**

by maximizing the energy according to the Adsorption Site Finder protocol.

Tensile pull-off measurements on bonding strength

The bonding between polydopamine and different hydrogels were measured by tensile pull-off (UMT; CETR). The tests were carried out using an aluminum mini pin stub (6.6 mm diameter; Ted Pella) and a glass or plastic (uv-transparent acrylic; Ted Pella) slide as the adherends under aqueous or wet conditions, with the hydrogels in between the adherends as the adhesive. Both adherends were coated with polydopamine and the appropriate guest molecules before joining. In a typical test, a solution of the hydrogels was spread onto the stub, which was then lightly pressed onto the slide and then the solution was cured *in-situ*. For the +Fe system, calcium alginate hydrogel networks were formed by adding 1 wt.% calcium carbonate (MQ200; EMD Chemicals) to 5 wt.% sodium alginate relative to water. After pressing the adherends together, this solution was then exposed to 0.1 M acetic acid for 1 hr to crosslink the gel solution (by dissolving calcium carbonate). For the +MBAA system, polyacrylamide hydrogel networks were formed by mixing 20 wt.% acrylamide, 3 wt.% polyacrylamide, 1 wt.% initiator (10% v/v of DEAP in

DMSO), and 1 wt.% N,N'-methylenebisacrylamide relative to water. After pressing the adherends together in deionized water, this solution was exposed to ultraviolet light (B-100PD UV-A Lamp; Spectroline) for 30 min to polymerize. In the case of acrylic adherend, we found the gel solution was not viscous enough to stay within the joint using the regular procedure; thus, the solution was concentrated to double the concentration and the polymerization occurred under more intense light. For the +diOH system, poly(vinyl alcohol) hydrogel networks were formed using an aqueous solution of 10 wt.% poly(vinyl alcohol) relative to water. Once the adherends were pressed together, they were stored in closed environment at 100% relative humidity. The poly(vinyl alcohol) jointed samples were then frozen at -10°C for 60 min and thawed at room temperatures (~23°C) for 60 min and this freeze-thaw process was repeated 5 times to turn the gel solution into a hydrogel. For the hybrid system, hybrid hydrogel networks were formed using a modified procedure based on the work of Sun and coworkers[8]. In short, 43 wt.% of acrylamide was dissolved in water, along with 0.025 wt.% N,N'-methylenebisacrylamide, 5 wt.% sodium alginate, 0.56 wt.% calcium carbonate, and 1 wt.% initiator, with all values relative to the weight of water. After pressing the adherends together, this adhesive joint was then exposed 0.1 M acetic acid for 1 hr, with the first 30 min of this time also exposed to ultraviolet light. For comparison, a cyanoacrylate-based underwater superglue (Two Little Fishes; CorAffix) was used. The adherends were then pressed together and immersed in deionized water for 1 hr. For the pull-off, a custom fixture with a nylon string was used to attach the stub to the tensile tester. The stub was then pulled away vertically from the slide, at a rate of 10 mm/min, until separation. Data for time, position, and force were recorded during the experiment.

Stretching of calcium alginate hydrogel on PDMS
To demonstrate the adhesion between calcium alginate hydrogel and plastics, a strip of PDMS (10:1 ratio, cured at 90°C for 90 min; Sylgard 184) was fabricated with an approximate dimension of 75 mm × 25 mm × 1.5 mm. To avoid the unintended spreading of alginate for the subsequent deposition of the gel solution, this strip was only coated in its center region by depositing 1 mL of the coating solution of +Fe for 15 min

on the strip's surface. After rinsing with deionized water and drying the strip, 1 mL of 1 wt.% sodium alginate mixed with 0.2 wt.% calcium carbonate was dropped onto the coated region. 6 µL of pure acetic acid was then deposited onto the surface of the alginate drop to start gelation. After waiting for 60 min under 100% relative humidity, the strip was stretched to ~40% strain to demonstrate the adhesion between the formed alginate hydrogel and the strip. For the uncoated case, the procedure was the same, except without the coating step, and with the alginate solution dropped directly onto the center region of the PDMS.

Shrinking of polyacrylamide hydrogel on polystyrene

To demonstrate the adhesion between polyacrylamide hydrogel and plastics, a small Petri dish (35 mm diameter, polystyrene; Fisher Scientific) was coated by filling the dish with the coating solution of +MBAA. After rinsing with deionized water and drying the dish, 2 mL of gel solution consisting of 40 wt.% acrylamide, 2 wt.% initiator, and 2 wt.% N,N'-methylenebisacrylamide relative to water was poured into the Petri dish. This solution was then exposed to ultraviolet light (B-100PD UV-A Lamp; Spectroline) for 30 min to crosslink. Afterwards, the Petri dish containing the polyacrylamide hydrogel was placed in a dust-free flow hood to dry the hydrogel overnight under room temperatures (~23°C). For the uncoated case, the procedure was the same, except without the coating step of the Petri dish. Sample images were taken before and after drying the hydrogels.

Bonding of artificial mussel byssus

To demonstrate the bonding of artificial mussel byssus with other surfaces, substrates including glass, polyvinyl chloride, mica, and aluminum, along with a bottle cap (polypropylene composite) were coated with the coating solution used for the hybrid hydrogel system. To form the artificial mussel byssus on the bottle cap, a disposable syringe (3 mL; BD) with the plunger removed was used as a mold for the gelation of the hybrid hydrogel. 2 µL of glacial acetic acid was first dropped with a micropipette into the mold, near the base of the syringe interior. After rinsing and drying the coated substrate, the syringe mold was clipped

onto the substrate. 1.5 mL of a hybrid hydrogel gel solution, same as the one used in the tensile pull-off tests, was then introduced to the bottom of this mold in contact with the substrate's surface. To gel, this solution was rested for 30 min for physical crosslinking, then exposed to ultraviolet light (B-100PD UV-A Lamp; Spectroline) for another 30 min for chemical crosslinking. Afterwards, the syringe mold was carefully removed from the coated substrate, leaving the hybrid hydrogel behind. This hybrid hydrogel was stretched to lift a soft drink bottle (610 g), with images taken for demonstration. For the pull-off measurement of the bonding strength, this hydrogel byssus was clamped 1.5 cm from the base and pulled vertically at 50 cm/min. The procedures for other substrates were similar, except for using a 1 mL syringe and 0.5 mL of the gel solution diluted twice with deionized water, for a better stretchability and a closer physical resemblance to that of real mussel byssus.

2.4 Formation and characterization of polydopamine co-deposited with "guest" molecules

We selected three common hydrogel systems, calcium-alginate, polyacrylamide, and polyvinyl alcohol, based on ionic, covalent, and physical crosslinking, respectively, for study. The guest molecules associated with the hydrogel systems are ferric ions (+Fe) for calcium-alginate, N,N'-methylenebisacrylamide (+MBAA) for polyacrylamide, and 2,4-pentanediol (+diOH) for polyvinyl alcohol. These guests resemble their respective hydrogels in either affinity or structure, and they interact non-covalently with polydopamine by varying degrees: the ferric ions form strong bonds by the well-established iron-catechol coordination[31] while the N,N'-methylenebisacrylamide and 2,4-pentanediol form weak bonds likely by a combination of hydrogen bonding, van der Waals, and π-interactions. For tuning the conformation of polydopamine, a relatively small quantity of guests is included in its deposition precursor solution. A typical deposition consists of immersing a substrate in a buffer solution (10 mM Tris at pH 8.5) containing dopamine, oxidant (ammonium persulfate), and guests for 15 minutes and then thoroughly rinsing the surface with deionized water to remove loosely bound components. The resulting polydopamine layer contained approximately 90% water by mass according to water content measurements (**Fig. 2.2**), a dry thickness of about 10 nm and correspondingly, a wet thickness of about 100 nm as indicated qualitatively by atomic force microscopy and X-ray photoelectron spectroscopy and quantitatively by areal density measurements (~0.01 g/m^2).
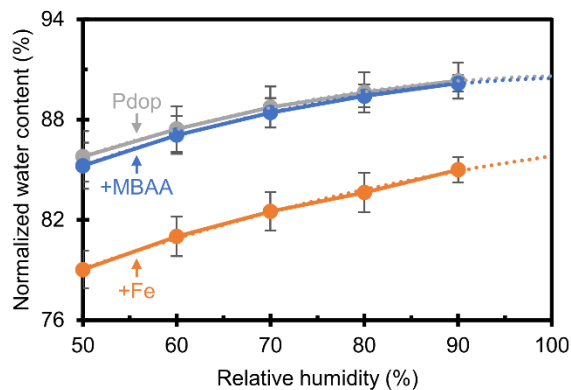
Fig. 2.2: Measured water content of polydopamine aggregates in equilibrium with relative humidity.

The normalized water content extrapolated to 100% relative humidity is equivalent to the water content of polydopamine in a fully hydrated environment. The error bars represent one standard deviation ($n \geq$ 3).

We investigated the influence of guests on polydopamine chemically by Raman spectroscopy, Fourier-transform infrared spectroscopy, and high-resolution X-ray photoelectron spectroscopy (**Fig. 2.3**) and physically by atomic force microscope and water contact angle measurements (**Fig. 2.4**). According to the chemical analysis, only the +Fe system demonstrated a detectable difference from that of pure polydopamine, showing a strong chelation between the ferric ions and catechol functional groups and an increased concentration of ferric ions in polydopamine. Even in this case, the covalent structure of polydopamine remained similar, with only minor shifts in infrared adsorptions, almost identical atomic ratios between C, O, and N, and notably the same high resolution C1s spectrum for the polymer backbones. This suggests that the presence of guests during deposition did not meaningfully alter the primary structure of polydopamine, which is anticipated from the non-covalent nature of the guest-host interactions. On the other hand, the physical analysis revealed a more pronounced effect, displaying visually different surface roughness and water contact angles among the different conditions. Considering the similarities in chemistry, we attribute that the main cause of these differences to changes in the

secondary/tertiary structures of polydopamine. This supports our premise of using guests to tune the physical conformation of polydopamine.
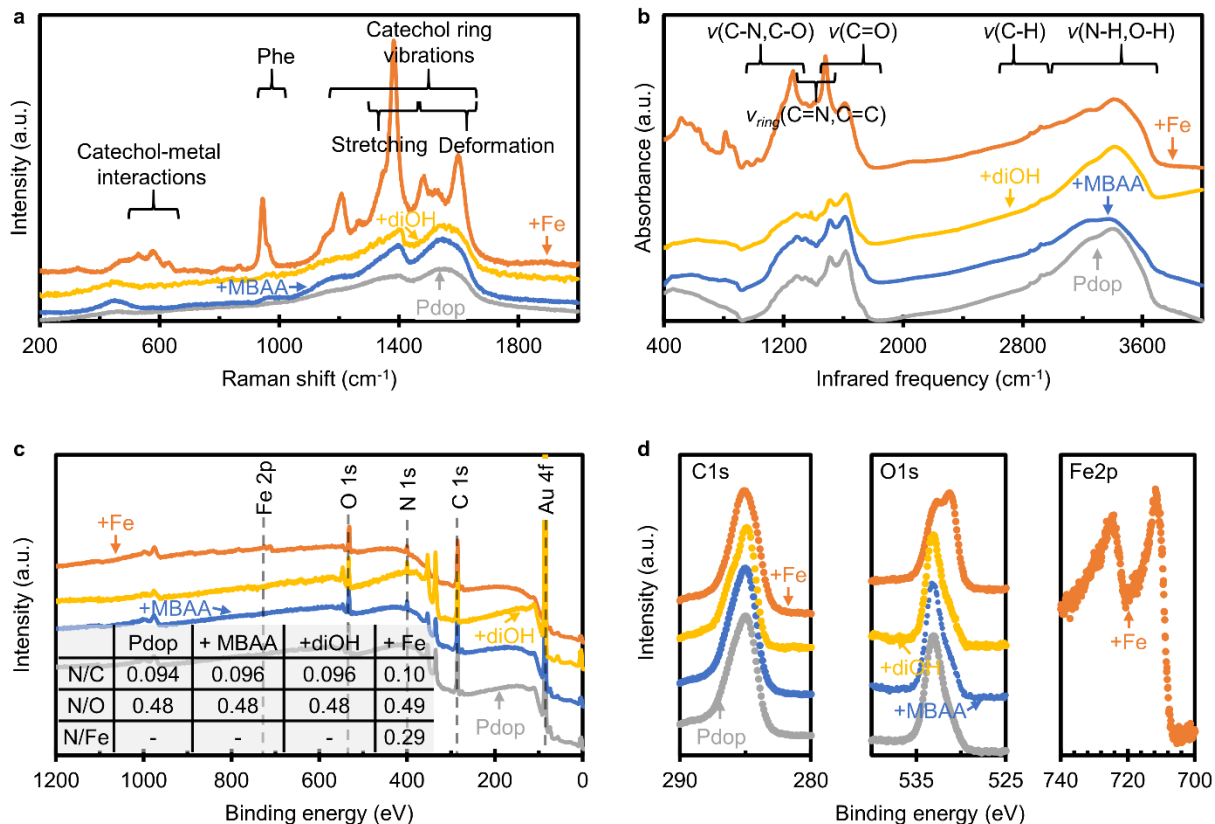
Fig. 2.3: Chemical characterization of polydopamine. a, Raman spectrum of polydopamine aggregates. **b**, Fourier-transform infrared spectrum of polydopamine aggregates. **c,d**, X-ray photoelectron survey (**c**) and high-resolution spectrums of C1s, O1s, and Fe2p (**d**) of polydopamine coatings coated on gold.
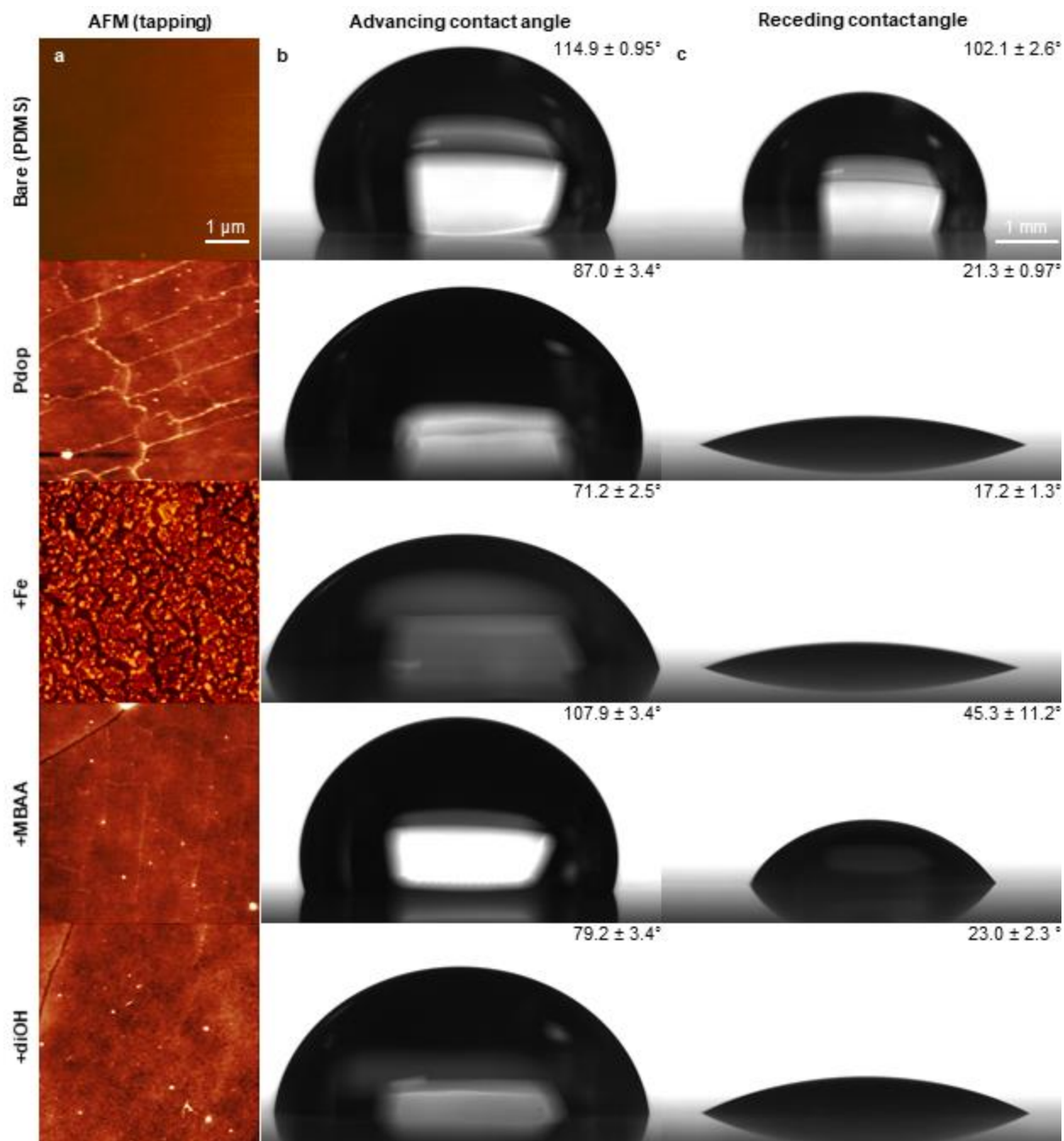
Fig. 2.4: Physical characterization of polydopamine. a, Atomic force microscopy scans on polydopamine coatings coated on PDMS; the cracks were caused by the drying of polydopamine and the large difference in stiffness between the coating and the underlying substrate, where the pattern of cracks reflects the physical structures of polydopamine. **b,c,** Advancing (**b**) and receding (**c**) contact angles of water on polydopamine coatings coated on PDMS. The error bars represent one standard deviation ($n \geq 3$).

2.5 Effect of molecular conformation on interfacial adhesion at the molecular and microscopic scales
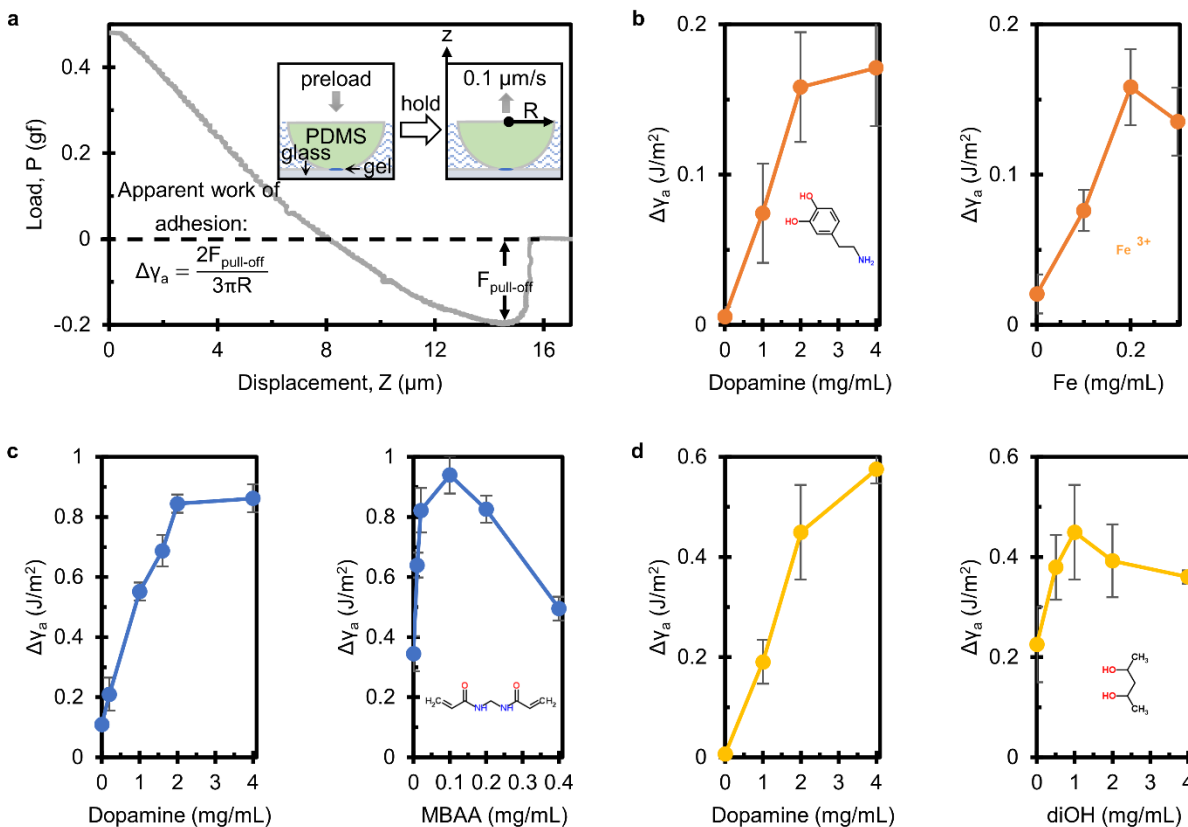
Fig. 2.5: Work of adhesion between polydopamine and gel solution. a, Typical load *vs.* displacement curve from separating surfaces in contact in micro-indentation measurements; the insert shows the schematic for the setup of the test; the apparent work of adhesion was calculated using the pull-off force according to JKR contact mechanics. **b-d**, Changes in the apparent work of adhesion with respect to increasing concentrations of dopamine molecules or guest molecules for the +Fe (**b**), +MBAA (**c**), and +diOH (**d**) systems. The error bars represent one standard deviation ($n \geq 4$ for minimum and maximum values and $n \geq 2$ for the rest).

We investigated the interfacial adhesion between polydopamine (+guest) and the corresponding hydrogel polymers by micro-indentation (**Fig. 2.5**). In these experiments, hydrogel solutions were sandwiched at a finite normal preload between a soft PDMS hemisphere and a rigid flat glass surface underwater, with

both surfaces coated with polydopamine (+guest) at varying deposition concentrations of dopamine and guest. To highlight the adhesive interactions between the hydrogel solutions and the corresponding surfaces, these solutions did not contain any crosslinkers to minimize cohesion and were given enough time to establish proper contacts with the surfaces. For the +MBAA system, acrylamide monomers were polymerized *in-situ* by ultraviolet excitation within the contact area. For all systems, the resulting interfacial adhesion between the hydrogel solutions and the polydopamine (+guest) surfaces was determined by measuring the work of adhesion for separating the surfaces. For all hydrogel systems, the work of adhesion increased asymptotically with respect to the concentration of dopamine and parabolically with respect to the concentration of guests at deposition. For the former, since the work of adhesion plateaued at about the same dopamine concentration regardless of the different hydrogel systems, the observed trend was likely intrinsic to the formation of polydopamine, presumably due to greater surface density of polydopamine at higher dopamine concentrations[41]. On the other hand, for the latter, the parabola indicated that there is an optimal guest concentration for adhesion, implying that it is likely a function of guest-host interactions. In the case of +Fe system, these interactions can be intuitively explained by chelation, where the presence of ferric ions during deposition leads to the conjugation and concentration of ferric ions in polydopamine (as confirmed by the chemical analysis), causing a stronger binding to alginate polymers *via* ionic bridging. Since catechol forms mainly tri- and bidentate chelates with ferric ions under the alkaline coating conditions[9,42] (which was evident from the bright red to dark purple complexation displayed during the deposition process), the dopamine molecules would polymerize around the ferric ions accordingly during deposition. This results in a molecular conformation of polydopamine that effectively "locks" the ions in place (as supported by both the physical and chemical analysis), leading to a stronger alginate binding. To confirm this, ferric ions were separately adsorbed on pure polydopamine coating; compared to the one-pot deposition, the resulting interfacial adhesion with alginate polymers was about 3 times weaker (**Fig. 2.6**).
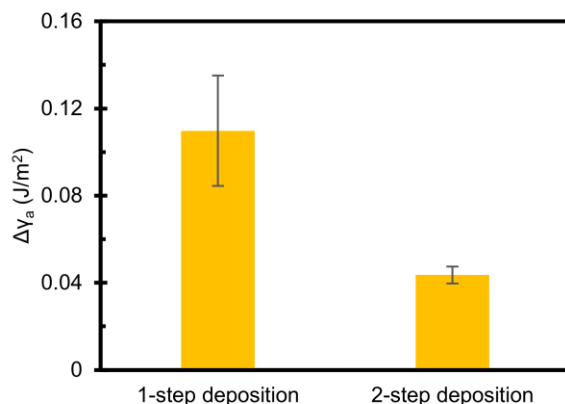
Fig. 2.6: Apparent work of adhesion between +Fe and alginate polymers. +Fe was formed by depositing ferric ions (0.2 mg/mL) in one step or in two steps with polydopamine. The error bars represent one standard deviation ($n \geq 3$).

In contrast to the +Fe system, the conformational changes for +MBAA and +diOH cannot be directly explored because of their significantly weaker interactions with dopamine. Accordingly, we carried out additional experiments to examine if other mechanisms are responsible for the increased adhesion. For the +MBAA system, the same experiment was repeated but with pre-polymerized polyacrylamide solution and without the use of ultraviolet irradiation (**Fig. 2.7**). The result showed a similar relative increase in adhesion for polydopamine (+MBAA) over pure polydopamine, suggesting that while covalent bonding is a possibility due to the radical polymerization of polyacrylamide, the increase in adhesion is likely a consequence of non-covalent interactions between polydopamine and polyacrylamide. The experiment was also repeated to explore the role of surface roughness, where polyacrylamide was sandwiched in between polydopamine (+Fe) surfaces (**Fig. 2.8**). The polydopamine (+Fe) was expected to have a larger real contact area than that of pure polydopamine, inferred from the higher roughness and thickness of the coating detected by the atomic force microscope in dry conditions and the greater size and number of polydopamine aggregations observed in wet conditions during the coating process. Despite that, the interfacial adhesion for +Fe was found to be slightly lower than that of pure polydopamine. While this outcome does not disprove that roughness plays a role in adhesion, it suggests that it is unlikely the sole

mechanism. For +diOH system, we repeated the same experiment with other alcohol molecules such as methanol and isopropanol (instead of 2,4-pentanediol) (**Fig. 2.9**). We found that these molecules did not notably affect adhesion, indicating a level of molecular specificity is at play.
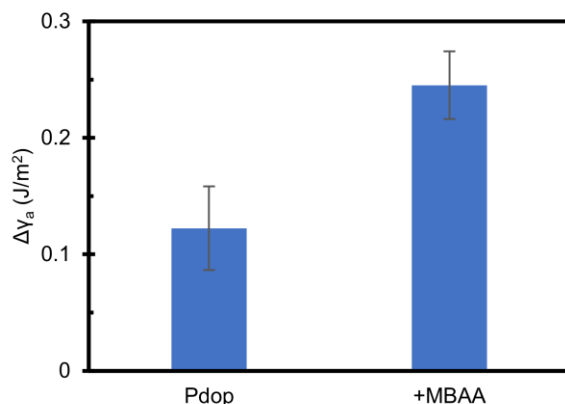
Fig. 2.7: Apparent work of adhesion between +MBAA and polyacrylamide polymers. +MBAA was formed by depositing MBAA (0.2 mg/mL) with polydopamine. The polyacrylamide polymers were pre-polymerized and ultraviolet irradiation was not used during indentation. The error bars represent one standard deviation ($n \geq 3$).
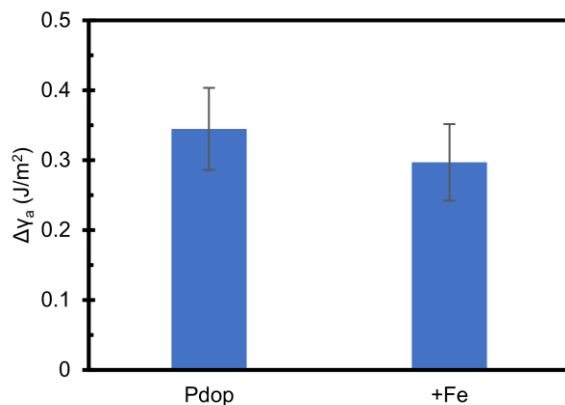

Fig. 2.8: Apparent work of adhesion between +Fe and polyacrylamide polymers. +Fe was formed by depositing Fe (0.2 mg/mL) with polydopamine. The error bars represent one standard deviation ($n \geq 3$).
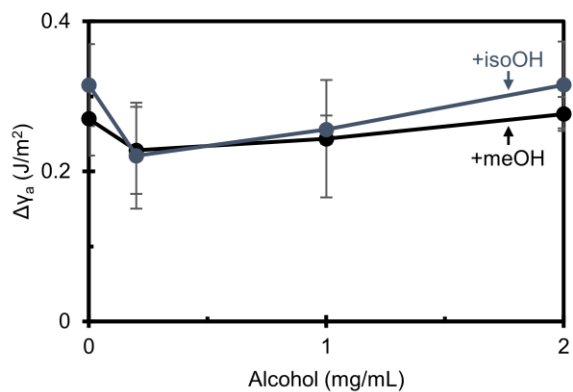
Fig. 2.9: Apparent work of adhesion between +isoOH or +meOH and polyacrylamide polymers at different alcohol concentrations. The error bars represent one standard deviation ($n \geq 2$).

To explore and confirm this molecular specificity, we investigated interactions at the molecular level by quartz crystal microbalance experiments and Monte Carlo simulations (**Fig. 2.10**). Considering the subtlety of the molecular specificity, it has been a challenge to quantify it at the molecular level even though we have made many attempts. Nevertheless, the QCM measurements and Monte Carlo simulations we have achieved so far do provide supportive evidences and scientific insights. In a typical test, the change in frequency (Δf) and dissipation (ΔD) of a quartz crystal coated with polydopamine (+guest) due to the presence of solutes in water was measured and compared to that of pure polydopamine. For the +MBAA system, polydopamine (+MBAA) showed higher affinity to the crosslinker of polyacrylamide hydrogels – demonstrating about 50% higher change in frequency and dissipation upon the adsorption of the solute. This result suggests that the mechanism behind the increase in the interfacial adhesion for the +MBAA system is likely related to molecular imprinting, where the removal of N,N'-methylenebisacrylamide molecules after the deposition of polydopamine leaves behind molecular imprints in the polydopamine. For the +diOH system, when polydopamine (+diOH) was exposed to 2,4-pentanediol, an "oligomer" of polyvinyl alcohol polymer, while the change in frequency were almost identical to that of pure polydopamine, there was a significant difference in dissipation. This behavior appeared to be selective as no change was detected when the surface was exposed to ethanol as a solute instead of 2,4-pentanediol,

indicating a molecular imprinting like behavior. Additional quartz crystal microbalance experiments might be needed to confirm these observations. To investigate the adsorption behavior at a larger scale, we also attempted to perform the same experiments with a dilute solution of the polymers instead of small molecules of the hydrogels. However, no meaningful change in response was detected even when comparing bare and coated surfaces, perhaps, due to the changes being masked by the effect of solution viscosity. Alternately, we resorted to Monte Carlo simulations with the OPLS3e force field[43]. Since polydopamine cannot be modeled due to the inherent complexity of its polymerization process, amorphous cells of the polyacrylamide and polyvinyl alcohol were constructed and the interactions of the cells' surfaces to different dopamine analogs were examined. Under the assumptions that these analogs represent some of the acknowledged structures and functionalities found on polydopamine surfaces and that the unoptimized and optimized interactions approximate the nonconformal and conformal binding, respectively, between polydopamine and the hydrogel polymers, the increase in binding energy due to molecular conformation was on average about 5 times for polyacrylamide and 1.5 times for polyvinyl alcohol. While the simulation was highly qualitative, this result indicates the increase in the work of adhesion from micro-indentation was reasonable as their values are on the same order.
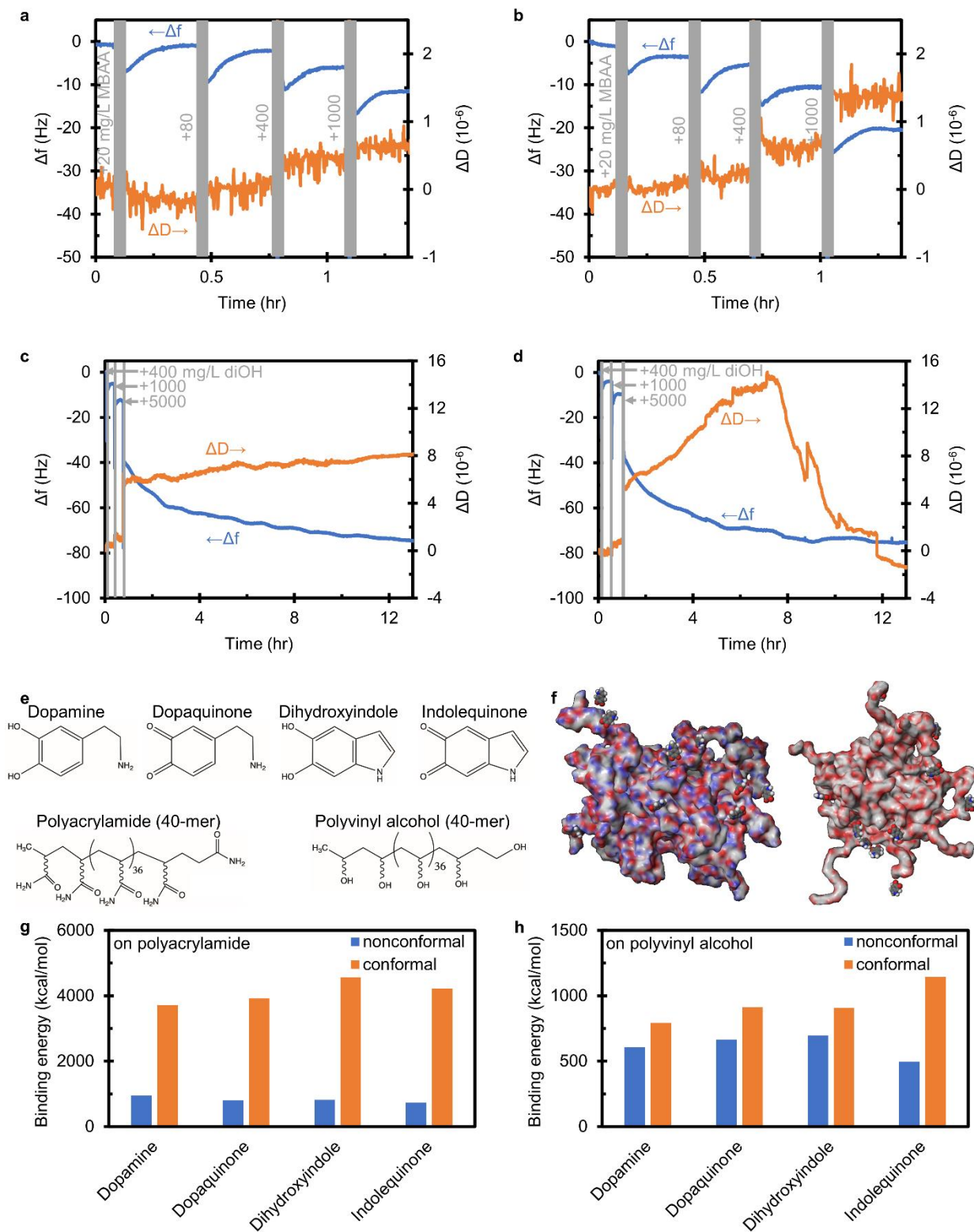
Fig. 2.10: Binding interactions due to conformation at the molecular level. a-d, adsorption of different

concentration of a solute on polydopamine under aqueous conditions measured by qartz crystal

microbalance for N,N'-methylenebis(acrylamide) on Pdop (**a**) and +MBAA (**b**) and for 2,4-pentanediol on

Pdop (**c**) and +diOH (**d**). The measurements were repeated 3 times (n = 3). **e**, Chemical structures of

molecules employed in Monte Carlo simulations. **f**, Typical physical system being simulated, where 10

molecules of a dopamine analog (*e.g.* indolequinone) interact with the surface of an amorphous cell (40

polymer chains at 1 g/cm^3) of polyacrylamide (left) and polyvinyl alcohol (right). **g,h**, Unoptimized and

optimized binding energy for the adsorption of different dopamine analogs to polyacrylamide (**g**) and

polyvinyl alcohol (**h**). Note that these binding energies are not true adsorption energies but rather a

comparative measure of the interactions since the simulation protocol employs a classical force field.

2.6 Effect of molecular conformation on adhesive strength at the microscopic and macroscopic scales
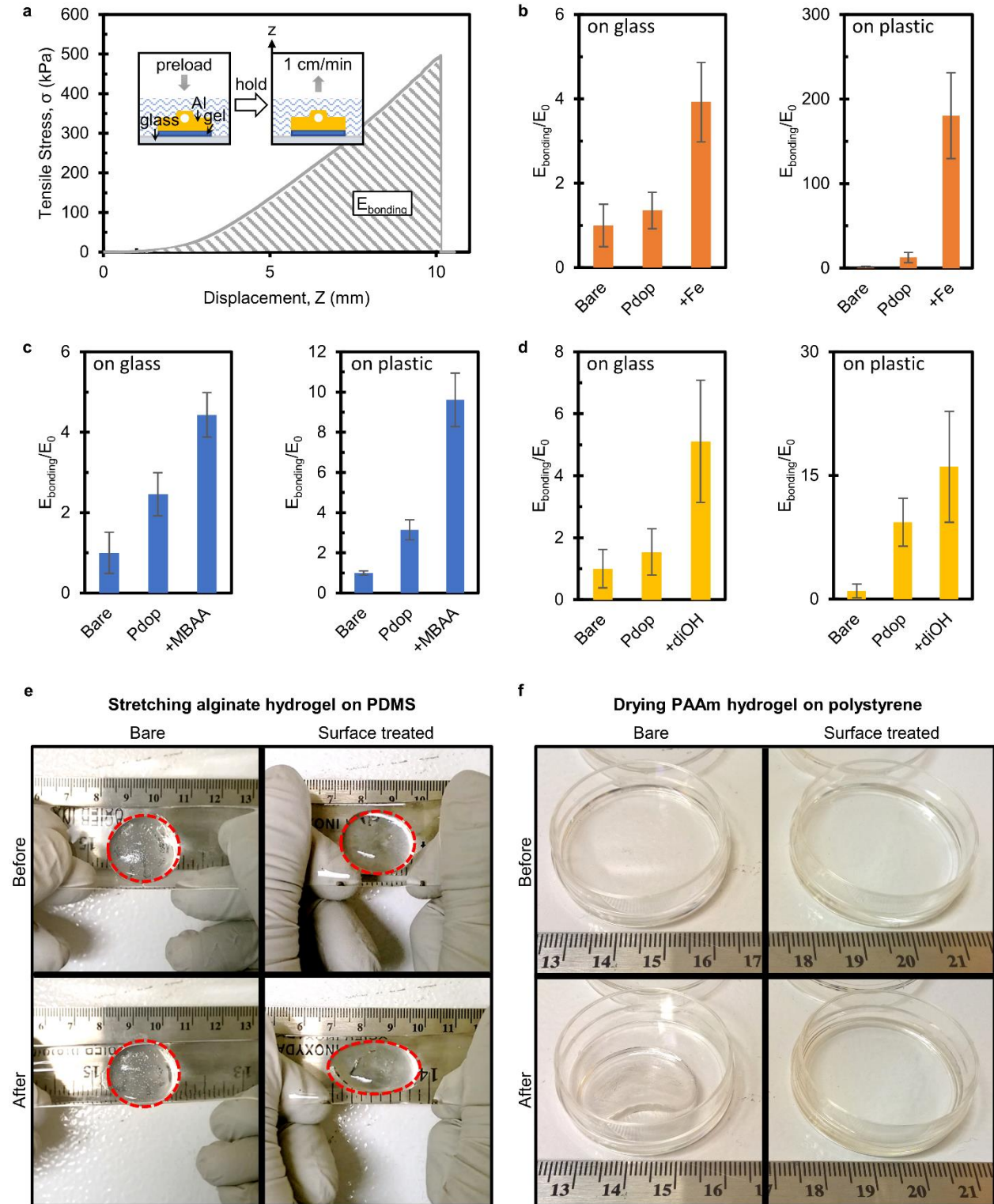
Fig. 2.11: Bonding strength of adhesive joints formed with polydopamine and hydrogels. a, Typical tensile stress *vs.* displacement curves in tensile pull-off measurements; the insert shows the schematic for the setup of the test; the apparent bonding energy was obtained by integrating the area under the curve. **b-d**, Effect of molecular conformation on the relative apparent bonding energy of the adhesive joints for the +Fe (**b**), +MBAA (**c**), and +diOH (**d**) systems. **e**, Demonstration of the bonding of hydrogels on plastics with and without the coating of conformed polydopamine; the presence of coating enhanced the bonding strength, enabling an alginate hydrogel to stretch along a PDMS strip (**e**) and a polyacrylamide hydrogel to withstand shrinkage when drying in a polystyrene petri dish. The error bars represent one standard deviation ($n \geq 3$).

To understand how these changes in molecular interfacial adhesion translate to macroscopic applications, we designed a set of tensile pull-off experiments to test the bonding of hydrogels with very different curing conditions or mechanical properties (**Fig. 2.11**). In a typical experiment, the hydrogel polymer solutions from the previously mentioned hydrogel systems were applied to bond two adherends together, aluminum on either glass or acrylic plastic. Once applied, the solutions were cured *in-situ*, where alginate was crosslinked by Ca^{2+}, acrylamide was crosslinked by N,N'-methylenebisacrylamide and ultraviolet irradiation, and polyvinyl alcohol was crosslinked by freeze-thaw cycles, forming gels with thickness on the order of ten microns. The joining processes for the former two hydrogel systems were performed entirely in a fully hydrated environment and the latter system was performed in 100% relative humidity. We attempted to also cure polyvinyl alcohol in fully hydrated environment using sodium tetraborate but found the cohesive strength of the resulting gel was simply too weak to provide satisfactory measurements. For quantitative analysis, we measured the bonding strength by pulling apart the joints, using the apparent bonding energy of the process for characterization. The bonding energies for adherends with no coating, with polydopamine, and with polydopamine (+guest) were compared with each other. Polydopamine (+guest) coating showed approximately a 2 to 3-fold increase in adhesion over

pure polydopamine, which is in good agreement with the micro-indentation and the simulation results. This correlation meets the expectation that due to hydrogels being largely viscoelastic, the energy is roughly a mathematical product between the energy dissipation caused by the bulk properties of hydrogels and their interfacial adhesion[44]. Comparing with bare surfaces, polydopamine (+guests) significantly improved bonding energy, with about half an order of magnitude increase on glass for all systems and with one order, one and a half orders, and two orders of magnitude increase on polystyrene for +MBAA, +diOH, and +Fe, respectively. The difference in increase between glass and plastic might be attributed to the high surface energy of glass and the low surface energy of plastics. This level of adhesion increase could potentially be useful for bonding hydrogels to other materials. For example, we found that we could stretch alginate hydrogel bonded on PDMS with more than 40% strain, while the control on bare surfaces failed to adhere without any external stress; additionally, we could prevent the peeling and shrinkage induced by drying for the polyacrylamide films coated on polystyrene Petri dishes, whereas the controls displayed a planar shrinkage of approximately 50% in area.
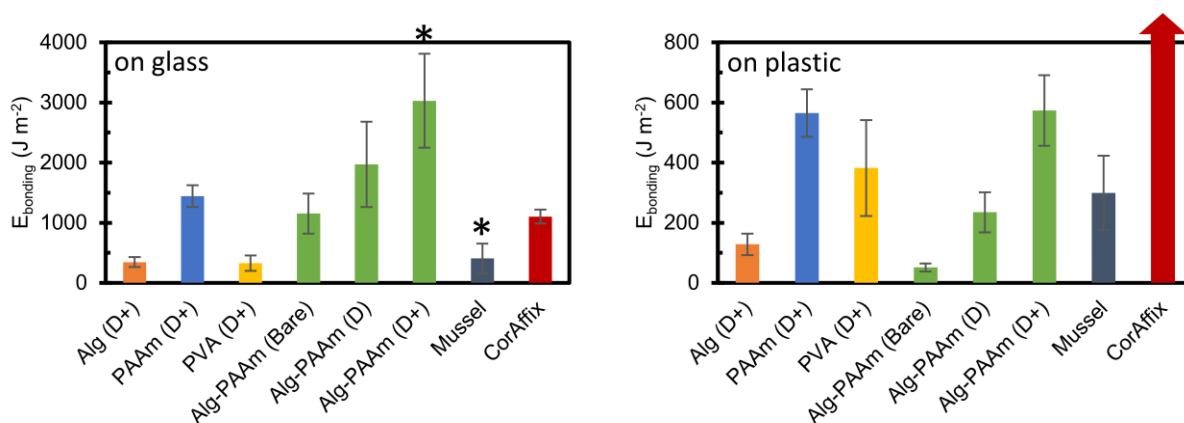
Fig. 2.12: Apparent bonding energy of adhesive joints formed by bonding aluminum on glass or on plastic with different hydrogels with and without polydopamine coatings underwater. Their performance was compared to the ones of natural mussel and commercial cyanoacrylate adhesive (CorAffix). The star (*) indicates cohesive failure of the joint and the arrow indicates an energy value far exceeds the range of the graph. The error bars represent one standard deviation ($n \geq 3$).

To further leverage this molecular recognition enhanced adhesion for practical applications, we exploit energy dissipation. As pointed out by other studies[45,46], the bonding of hydrogels requires not only strong adhesion at the interface but significant energy dissipation from the bulk of the hydrogels – generally, tough bonding needs tough hydrogels. In this case, we formulated a tougher hydrogel, inspired by the work on highly stretchable hydrogels[8], by combining calcium alginate and polyacrylamide. Subsequently, we applied this gel to form a tough joint between aluminum and either glass or acrylic plastic (**Fig. 2.12**). On glass, the bonding energy of this joint is significantly stronger, at least doubled, than that of either alginate or polyacrylamide hydrogel individually, possibly due to the gel's tough and stretchable nature. On plastic, while the bonding energy of the hybrid hydrogel is significantly higher than that of alginate, it is about the same as that of the polyacrylamide hydrogel. Comparing this performance to that of the mussel, which inspired the polydopamine coating, the bonding energy on plastic is on the same order of magnitude for both the mussel and hybrid hydrogel, but on glass, the bonding energy of the hybrid hydrogel (even without surface treatment) is significantly higher. The above results are likely due to the hybrid hydrogels being tougher, combined with the mode of failure of the joints, where the hybrid hydrogel, polyacrylamide, and mussel all failed adhesively on plastic and cohesively on glass (for mussel, the failure is adhesive, ~94%, on acrylic and cohesive within the plaque-thread, ~91%, on glass). Comparing the performance of the hybrid hydrogel joint to commercial cyanoacrylate based underwater superglue (CorAffix by Two Little Fishes), the hydrogel joint outperformed the commercial superglue on glass by 3 folds, but was significantly outperformed on plastic by one and half of orders of magnitude. We attribute this result to the fact that cyanoacrylate only forms physical bonds with glass but can form strong chemical bonds with plastics. In comparison, our polydopamine (+guests) forms physical bonds with both substrates by non-covalent adhesive interactions offered by mussel chemistry. Thus, it is not surprising to see that the hybrid joint outperforms cyanoacrylate superglue on glass but not on plastics underwater.

Although the absolute performance of the hybrid hydrogel on the acrylic plastic is weaker than that of on glass, the relative improvement over uncoated surfaces is much greater — about an order of magnitude.

The hybrid hydrogel also enabled us to demonstrate large-scale adhesion and dissipation. In nature, the mussel byssus bonds to surfaces by non-covalent interactions at the interface and bulk energy dissipation from its plaque and thread[47,48]. To this end, we molded the hybrid hydrogel into the shape of mussel byssus in contact with various substrates and quantitively measured its performance on an everyday plastic bottle cap (**Fig. 2.13**). The result tends towards larger variance, perhaps due to the varying quality of contact with the substrate during plaque formation. For the stronger joints, we found that we can dangle a bottle of soft drink with the hydrogel byssus. In general, the stress-displacement curve of the artificial mussel byssus demonstrated that by having the shape of the mussel byssus and the toughness of the hybrid hydrogel, we can amplify the gain from interfacial adhesion by energy dissipation from the byssus, resulting a much higher bonding energy per bonding strength (in comparing D, pure polydopamine, and D+, polydopamine (+guest), double the bonding strength translates to an order of magnitude increase in bonding energy). The overall results demonstrate that the polydopamine (+guests) coupled with good energy dissipation could potentially be used in the assembly and construction of soft robotic devices and biomedical sensors, which require good mechanical integrity and durability, as well as flexibility of the joints.
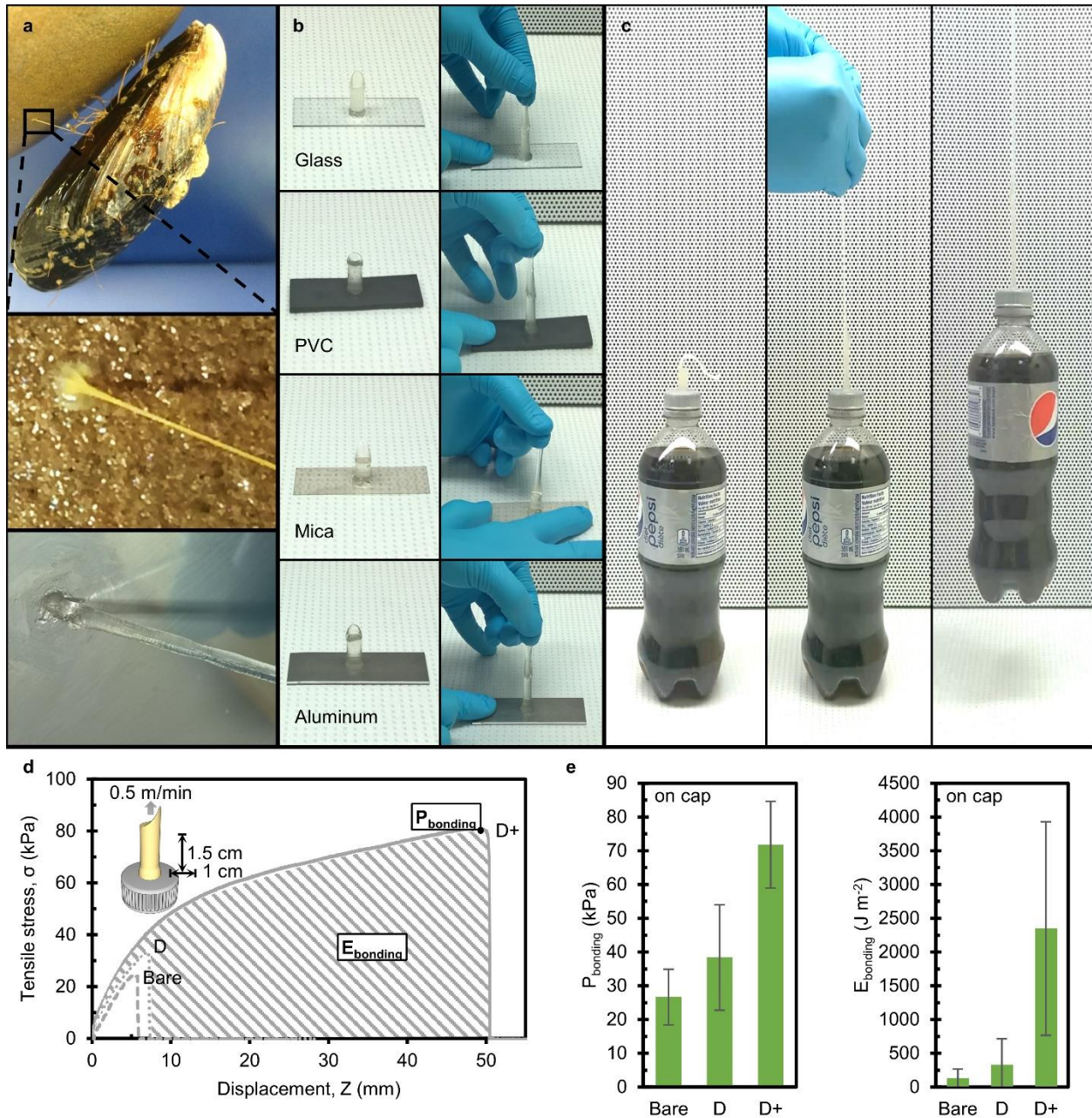
Fig. 2.13: Joining of hydrogel 'artificial mussel byssus' to other materials. The byssus was formed by molding and curing a hybrid stretchable hydrogel consisting of polyacrylamide and alginate on the bottle cap (which was made of polypropylene composite). The interfacial adhesion between the hydrogel and the substrate was enhanced by a polydopamine (+crosslinker) layer of 100 nm in thickness. **a**, The artificial byssus mimics the one from natural mussel in both shape and mechanics. **b**, Photos showing artificial mussel byssus adhering to different substrates: examples shown are glass, PVC, mica, and aluminum. **c**,

Demonstration of 'artificial mussel byssus' lifting a bottle of soft drink (with a total weight of 610 g). **d**,

Typical tensile stress vs. displacement curves for the detachment of the byssus from the cap; the insert

shows the schematic for the setup of the test; the apparent bonding strength is the maximum tensile

stress detected and the apparent bonding energy was obtained by integrating the area under the curve.

e, Effect of molecular conformation on the relative apparent bonding strength and bonding energy of the

byssus. The error bars represent one standard deviation ($n \geq 3$).

2.7 Concluding remarks

Overall, in this chapter, we manipulated the molecular conformation of polydopamine by including non-covalently interfering guests during its formation, thereby imparting a molecular memory towards specific hydrogels. Three common hydrogel systems, calcium-alginate, polyacrylamide, and polyvinyl alcohol were selected for this study. The guest molecules corresponding to the hydrogels were ferric ions, N,N'-methylenebisacrylamide, and 2,4-pentanediol, respectively. The use of guests results in substantially stronger interfacial adhesion (a several fold increase) between all hydrogel systems and the polydopamine surface across a broad range of length scales, drawing a general connection between the molecular conformation in biology and micro- and macroscopic adhesion in materials science. As the structure of polydopamine is highly disordered and nonspecific for the conformational changes, we expect the underlying concept of imparting "memory" could be extended to other material systems, providing a facile strategy for enhancing interfacial adhesion and bonding.

Chapter 3. A Hybrid Material that Reversibly Switches between Two Stable Solid States: Fundamental and Applications[1]*

3.1 Summary

Most solid matter has a single stable solid state for a particular set of conditions. Nonetheless, materials with distinct, interchangeable solid states would be advantageous for several technological applications. Here, we describe a material composed of a polymer impregnated with a supercooled salt solution termed as sal-gel, that assumes two distinct but stable solid states under the same range of temperatures (-90 to 58°C) and pressure. Upon transient stimulation of nucleation, the material switches from a clear and soft solid to a white and hard state, which can be 10^4 times stiffer than the original (15 kPa *vs.* 385 MPa). This hard solid becomes soft again by transient heating, demonstrating the reversibility of the transition. This concept, exploiting the robust physical metastability of a liquid state, is extended to sugar alcohols, resulting in a stimuli-responsive and non-evaporating sug-gel. These "two-in-one" solid materials may find potential uses in soft robotics and adhesive applications.

3.2 Introduction

The balance between shape adaptability and load-bearing capability represents a common compromise in engineering design. Nature resolves this dilemma with mechanical duality, allowing a single material to reversibly switch between soft and hard states. For instance, Echinoderms such as sea cucumbers have mutable connective tissues (dermis) that can alter their mechanical properties between a soft state for dexterity and locomotion and a rigid state for safety and protection[49]. This duality is highly desired in many technological areas associated with: soft robotics for reversibly switching from softness for adaptability to hardness for precise movements, adhesion and adhesives for balancing between softness for good contact and rigidity for resisting fracture at the interface, and other advanced applications such as enabling wing morphing to improve flight performance in aeronautics[50].

To meet the demand of mechanical duality, significant efforts have been made over the years for developing smart materials with switchable stiffness[51,52], utilizing mechanisms such as swelling[53–55], first-order (*e.g.* melting)[56] and second-order phase transitions (*e.g.* glass transition)[53,57], and surface polarization[58]. For example, Capadona *et al*. have created a sea cucumber-inspired stimuli-responsive polymer nanocomposite containing rigid cellulose nanofibers with hydrogen bonds that can be switched on and off by desorbing and absorbing of water, respectively[53]. By additionally contrasting the polymer network above or below its glass transition temperature, this nanocomposite can achieve a significant change in stiffness of more than 10^3 times. A key limitation for these smart materials has been that one of the mechanical states needs continual exposure to stimuli such as osmotic pressure (*i.e.* swelling by absorption of liquid)[53–55], heat[53,57], or electrical potential[58] to maintain this state. This persistence of stimulus would also place the material in a different environment, which can be subtle. For instance, the signaling of calcium ions during the contraction of skeletal muscle causes the condition of the muscle to change compared to that during relaxation. This requirement restricts the applicability of these materials, especially for those dependent on osmotic pressure as swelling usually causes the volume of the material

to change significantly (typically >30%). Overcoming the above limitation necessitates a material possessing two reversibly switchable solid states that each can exist under the exact same environment, such that the states are stable without stimulus (*i.e.* an external stimulus is only needed to trigger the switching but not for maintaining the states). Herein, we term this type of material a "two-in-one" solid.

One solution for creating "two-in-one" solids is to exploit mechanical (*i.e.* structural) metastability. This is exemplified by mechanical metamaterials (*e.g.* origami- and kirigami-inspired)[59–61] which can transform their stiffness – for instance, by changing topological states[60]. However, since these metamaterials are structure-based, they are inherently anisotropic, relatively difficult to fabricate, and can be prone to failure. Another solution is to exploit chemical metastability *via* the state of art of polymer science. Worrell *et al.* created a covalently cross-linked polymer network that can stably switch between dynamic and permanent crosslinks, correspondingly resulting in a fluid state or a solid state[62]. However, this switching was unidirectional. Gu *et al.* utilized networks of polymer-linked metal-organic cages in which the cages or junctions change shape and size on irradiation[63]. While these changes allowed the polymer to reversibly switch its network structures, the resulting change in stiffness was one order of magnitude and the junctions would degrade over switching cycles. In this work, we demonstrate that physical metastability (*e.g.* supercooling) can be exploited to achieve dual stable and reversible solid states. This solution enables the creation of a non-structure-based material with multiple orders of magnitude difference in stiffness, representing an advance over previous works.

Supercooled salt ✚ Polymer network ═ Sal-gel

a

Potential energy

- Frozen salt
- Melted salt
- Polymer network

Nucleation

Energy barrier

Heat

Rigid solid

Soft solid

Reaction pathway

b

Soft state (E ≈ 10^4 Pa, 21°C)

Touch of seed crystals

> 58°C

Rigid state (E ≈ 10^8 Pa, 21°C)

2.5″   0.5″
2.5 mm

c

Material behavior at rigid state

High Polymer Content

Deform (↻ 360°)

Relax

Low Polymer Content
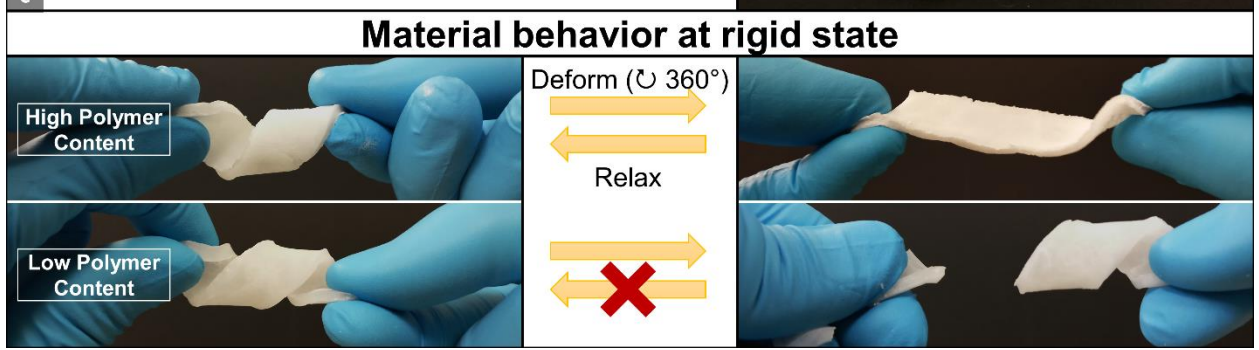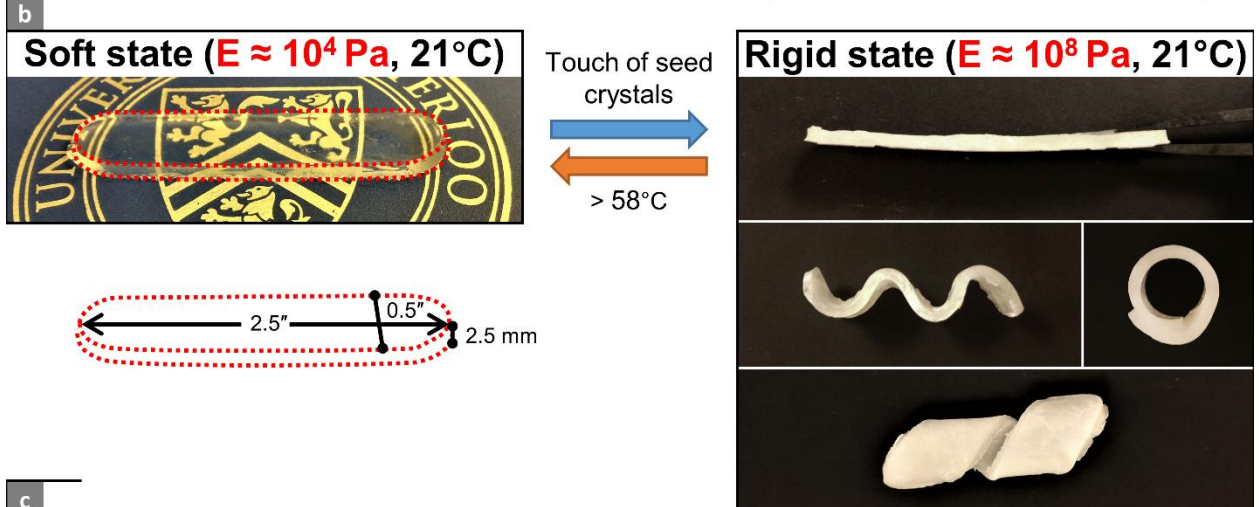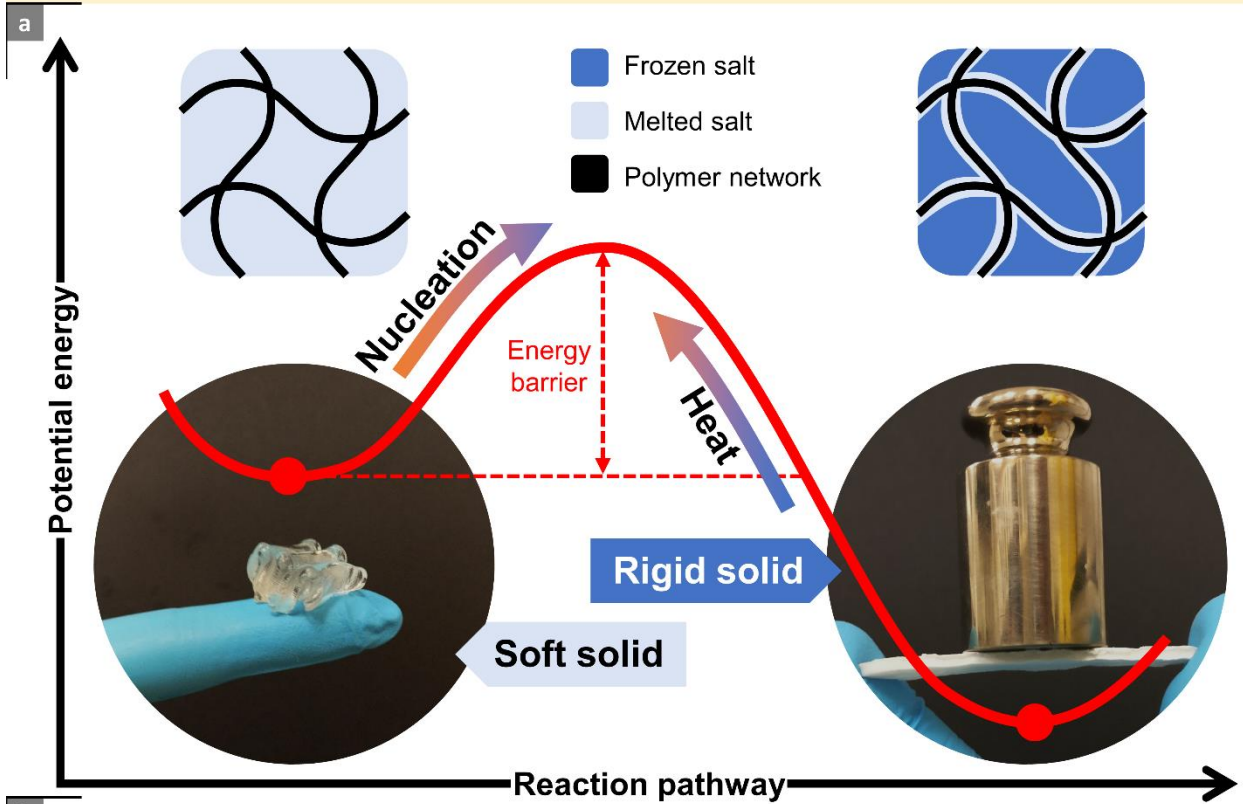
Fig. 3.1: Material behaviors of sal-gel. a, A plot of potential energy *vs.* reaction pathway, showing an energy barrier between two stable solid states with mechanical contrast; the squares on top depict the conceptual molecular portraits of sal-gel, where the salt is melted in the soft state and frozen in the rigid state; the circles at the bottom show the material behaviors of sal-gel, which is soft enough to be folded onto itself in the soft state and stiff enough to hold a weight of 200 g in the rigid state. **b**, On-demand shape-fixing of sal-gel (P10L10) by manipulating its shape in the soft state and then fixing the shape by touching the gel with salt seed crystals; the fixed shape can be reversed by heating the gel (>58°C). **c**, The fixed shape is rigid and inflexible when the polymer content of the sal-gel is low (P10L10) and breaks upon twisting; it is elastic and flexible when the polymer content is high (P30L10) and deforms when twisted but returns to the original fixed shape when released.

To obtain dual stable states, the underlying mechanism must have an energy barrier between the states, with each state resting at an energetic minimum (**Fig. 3.1a**). Crystallization of liquid can meet this requirement. To crystallize, the liquid initially requires the formation of a sufficiently large cluster of crystalline atoms or molecules, for which the free energy gain of transforming to the stable crystalline phase must overcome the free energy cost of creating an interface between the liquid and the crystal[64]. Consequently, reaching a critical cluster size can be very difficult, effectively creating an energy barrier and allowing the liquid to exist in a metastable state of supercooling or oversaturation, without yet crystallizing. This energy barrier can reliably be overcome *via* self-assembly — which can be induced by secondary nucleation (*e.g.* by the touch of a seed crystal)[65–67] — for liquid-to-crystalline and *via* heat for crystalline-to-liquid. Sodium acetate trihydrate, a phase-change material commonly known as "hot ice" (due to the heat released during freezing), is well-known for its ability to supercool; despite having a melting point of 58°C, it can remain stable as a supercooled liquid at room temperatures for years such that it has been used for seasonal energy storage[68,69]. A key prerequisite for "two-in-one" solids is that the transition between the states at the molecular levels should be insensitive to material's macroscopic

deformations. This prerequisite is generally difficult to attain for pure solids (for which both the crystalline and non-crystalline states are solid) because their molecular transition and alignment are intertwined. A classic example of this is natural rubber, where stretching reduces conformational entropy and crystallizes the polymer, which reverses back to its amorphous state upon relaxation[70]. On the other hand, liquids can meet this prerequisite because their molecules are more mobile, so that their microscopic order is insensitive to disturbances in their macroscopic order (*e.g.* pouring and stirring of a sufficiently supercooled liquid does not cause the liquid to crystallize).

Fundamentally, phase-change materials have the greatest potential for creating smart solids with large transformations in stiffness; going from solid to liquid, with the lowering of molecular connectivity occurring throughout the entire material, results in an almost infinite change in modulus. However, to be usable, a phase-change material must integrate with other materials for containment while in its liquid state. To date, proper integration of phase-change materials to fully realize their potential has not been attained. Typically, containment by compartmentalization with polymeric materials is utilized to construct large-scale engineered devices and structures[71–73]. However, this breaks the continuity of the phase-change materials at the macroscopic level, resulting in constructs that are mechanically anisotropic and potentially have more structural weaknesses. On the other hand, for integration as a polymer composite that is mechanically isotropic, the performance achieved so far is rather limited, especially considering the potential of infinite modulus change. For example, Van Meerbeek *et al.* have fabricated a bicontinuous metal-elastomer composite with an associated change in modulus of 31 times[56]. The central problem of integration lies in the incompatibility between the polymer and the phase-change material. Considering the most popular phase-change material for changing stiffness[51], low-melting point metal alloys, this incompatibility originates from the high disparity between the surface tensions of the components (typically on the order of N/m for metals *vs.* 0.01 N/m for polymers), making them thermodynamically unfavorable to mix. This leads to two undesired and contradictory concerns. Firstly, creating a continuous

network of metal in polymer (which is important for stress transfer) *via* direct mixing is problematic, since attaining percolation is already very difficult[74]. To create a continuous network, the polymer has to be made into a foam before introducing the metal[56]. This significantly limits the processability of the composite (*e.g.* for 3D printing). Secondly, if the melted phase-change material is continuous, it is likely to be squeezed out from the polymer matrix upon mechanical deformation[75].

Sodium acetate trihydrate can interact strongly with hydrophilic polymers due to its polarity and hydrogen bonding capability in addition to its supercooling effect, allowing us to reconcile and overcome the above concerns. In this work, we turned this phase-change material into a gel by polymerizing and crosslinking acrylic acid monomers *in-situ*, so the phase-change material can behave like a solid even in its liquid state. Using the Flory-Huggins theory, we estimated the compatibility of acrylic acid or poly(acrylic acid) (*i.e.* the solutes) with melted sodium acetate trihydrate (*i.e.* the solvent) and calculated[76] that the components are miscible with each other based on the free energy of mixing, ΔG_{mix} (**Supplementary Note 3.1**). Moreover, ΔG_{mix} is also the driving force behind swelling, where $\Delta G_{swell} \approx \Delta G_{mix} + \Delta G_{elastic}$. Provided that the polymer network has not already been stretched to its limit ($\Delta G_{elastic} \gg 0$), the gel can swell to accommodate the migration of liquid relative to the network and prevent the liquid from being squeezed out. On the other hand, the high compatibility also means that the same polymer network can hold a larger amount of phase-change material, enabling us to fully leverage the phase-change material's properties.

Overall, the above concepts condense into an elegant solution for creating materials with dual stable, reversible, and magnitudinally different solid states. By turning a supercooled liquid into a gel, we produced a moldable, printable, and light-weight ($\rho \approx 1.35\rho_{H_2O}$) hybrid material, sal-gel, that can interchangeably switch its effective stiffness without requiring constant stimulation (**Fig. 3.1a**). The molecular-scale integration allows us to fully leverage the phase transition and metastability of the salt,

such that the material is rubber-like while melted, yet its switching of states is largely, if not completely, independent of deformations, enabling on-demand shape-fixing (**Fig. 3.1b**). The resulting change in stiffness can be more than 10^4 times. This is highly desirable for "two-in-one" solids and to the best of our knowledge, rivals or exceeds that of other stiffness-changing materials including engineered devices[71,72,77–82]. To illustrate this, we plotted the maximum reported stiffness change against an estimated length scale of connectivity for various categories of materials/devices (see **Fig. 3.3g**). This connectivity length scale is considered as the minimum length that the connections responsible for stiffness switching operate on; at any smaller length scale, these connections will not function, imposing a theoretical limit to how far down these technologies can be scaled (**Supplementary Note 3.2**). This is especially relevant in the face of today's ever-growing demand for miniaturization and increasing performance density, where both size and weight of materials are at a premium.

3.3 Methodology, materials and characterizations

Preparation of sal-gel

Acetic liquid was prepared by mixing acetic acid (Glacial; Fisher Scientific) and deionized water at a mole ratio of 1:3 (to mimic the salt hydrate's molecular formula). A supercool salt stock solution was prepared by mixing the acetic liquid and sodium acetate trihydrate (ACS; VWR Analytical) at a weight ratio of 10:100 and heating this mixture at 90°C for at least 72 hours (to fully melt all crystallites). Polymer precursors were prepared by mixing acrylic acid (low water content, with 200 ppm 4-methoxyphenol as inhibitor, 99.5%; Alfa Aesar) monomer and N,N'-methylenebis(acrylamide) (99%; Sigma-Aldrich) crosslinker at a weight ratio of 100:5 for any data associated with **Fig. 3.3**, **Fig. 3.5**, and **Fig. 3.8** (for less variance in the rigid state and faster curing), and 100:1 for any data associated with **Fig. 3.1** and **Fig. 3.7** (for easier manipulation in the soft state).

Sal-gel was prepared by mixing acetic liquid, salt stock solution, and polymer precursors at 90°C. Once the resulting mixture was homogeneous and clear, 2,2-diethoxyacetophenone (>95%; Sigma-Aldrich) initiator was added to the mixture at a weight ratio of 1:100 relative to the monomer. The final mixture was kept at 90°C for an additional 10 minutes to remove bubbles and was then cured by irradiating with an ultraviolet light source (365 nm, LED floodlight BigBeam; Labino) at a 10 cm distance for 5 min under room conditions. Samples were then cooled to room temperature (approximately 21°C) before use.

Different compositions of sal-gel were made, denoted by P#L#, where P# is the weight percentage of monomers and L# is the weight percentage of acetic liquid, each relative to the salt hydrate. For example, for P10L10, the weight ratio between the monomers, acetic liquid, and salt hydrate is 10:10:100, respectively. Samples without polymers (P0L#) were simply referred to as L#. For fabrication of P5L5, a separate salt stock solution of 5:100 ratio of acetic liquid to salt hydrate was used.

Fourier-transform infrared spectroscopic measurement

For the sal-gel sample, the poly(acrylic acid) gel was prepared by removing the salt from P10L10 sample (with a 100:5:1 monomer to crosslinker to initiator ratio) through multiple exchanges with deionized water. For the pure gel sample, the same gel formulation as P10L10 was used, except both the acetic liquid and salt hydrate were replaced with the equivalent weight of deionized water. Both gel samples were dried, crushed into powders, pressed into pellets with potassium bromide (Infrared; Fisher Scientific), and then measured by Fourier-transform infrared spectroscopy (Nicolet 520; Thermo Fisher).

Indentation testing (Fig. 3.3 and Fig. 3.8)

All samples were prepared by forming sal-gel in a 20 mL glass scintillation vial. The amount of all components used was scaled around 10 g of salt hydrate. Tests were performed using a universal materials tester (UMT; CETR) by indenting on the flat surface of sal-gel in the melted and the frozen states with a hemispherical glass probe (3 mm radius). For each test, the probe was carefully brought into contact with the sample, and then indented into the sample at a rate of 0.05 mm/s to a depth of 0.5 mm, held for 10 sec (to give the sample time to relax) at that position, and then lifted 1 mm up at the same speed. Afterwards, the probe was immediately re-indented under the same conditions (to the same depth and on the same location). Force, time, and displacement information was recorded. Effective elastic moduli were extracted from the data using Hertzian contact mechanics, as detailed in **Supplementary Note 3.3**. Elastic contribution of the material response for the first indent was estimated by dividing the maximum compressive force measured from re-indentation over the maximum force from the initial indentation.

For melted samples, 5 μL of deionized water was placed on the tip of the probe before indentation (to minimize the effects of adhesion between the glass and the gel surface). Samples without polymers were only tested while frozen. Frozen samples were prepared by touching samples in the melted state with salt and leaving overnight to freeze (for consistency across samples with different freezing rates) in a closed environment. For freeze-thaw cycled tests, samples were indented first in the melted state and then in

the frozen state per cycle for a total of 5 cycles. To switch the states, the samples were either touched by salt and left in room conditions for 1 hour to freeze or heated at 90°C for 30 min and left in room conditions for 30 min to melt. To measure effect of temperature on the elastic modulus of sal-gel, P10L10 samples in the melted or in the frozen state were heated to 30, 40, and 50°C using a water bath. Indentations were performed after the samples had been stabilized at the target temperature for 15 minutes.

Tensile testing (Fig. 3.4)

All samples were molded into a dogbone shape (dimensions shown in **Fig. 3.4**) using a custom polydimethylsiloxane mold. Tests were performed using a universal materials tester (UMT; CETR) by gripping the samples at their shoulders and pulling at 10 μm/s to failure. Force, time, and displacement information was recorded. The dimensions at the gauge section (15 × 5 × 2 mm) were used to convert the force and displacement data into engineering stress and strain.

Frozen samples were prepared by touching samples in the melted state with seed crystals at the ends of the dogbone and leaving overnight to freeze in a closed environment.

Structural analysis of crystallization (Fig. 3.5)

Crystallization of P10L10 was visually inspected using both a regular camera for the macro-scale and a portable microscope (AM4113ZTS; Dino-Lite) for the micro-scale. The sample was touched with a salt crystal to initiate freezing and heated at 90°C for 30 min to melt. Additional observations were made for other samples (*e.g.* from indentation) during freezing.

Kinetic analysis of crystallization (Fig. 3.5)

1 mL of sal-gel samples were prepared *in-situ* in 1 mL syringes (NORM-JECT; Henke-Sass-Wolf), where the samples were cured through the syringe walls by ultraviolet irradiation and were cooled down to room temperature before measurements. The syringes were pre-marked at two points set at a known distance

apart. Crystallization was initiated by touching the sal-gel at the syringe tip with salt and a stopwatch was used to measure the time of the lead crystal to travel between the two points. The crystallization speed was calculated by dividing the distance over the measured time.

Thermal analysis of crystallization (Fig. 3.5)

Samples were prepared by touching melted sal-gel with salt and left overnight to freeze in a closed environment. For each test, about 10-20 mg of each sample was broken off, then transferred to and sealed in an aluminum hermetic pan. These samples were then analyzed using a differential scanning calorimeter (Q2000; TA Instruments). For each test, the sample was equilibrated at 10°C, then heated to 90°C at a heating rate of 5°C/min. The sample was held at 90°C for 10 minutes, then cooled to -90°C (using a cooling rate of 5°C/min up to -75°C, then 2°C/min from -75°C to -90°C). The sample was kept at -90°C for 10 minutes, then heated back up to 90°C (with a heating rate of 2°C/min up to -75°C, then 5°C/min up to 90°C). Finally, the sample was cooled back down to 10°C at 20°C/min.

For samples without polymer, 10 µL of melted solution was dropped into an aluminum hermetic pan, and frozen *in-situ* (except for the acetic liquid; this was to ensure accurate distribution of liquid and solid), then sealed.

Sal-gel demonstrations (Fig. 3.1 and Fig. 3.7)

Sal-gel samples were formed in a custom-made Teflon mold (with a slot composed of a rectangular area of 0.5" × 2" in dimensions at the center and two semicircular areas of 0.5" in diameter at the ends), where the mold and gel solution were both heated to 90°C before ultraviolet-curing under room conditions. Hands were wetted during handling of the samples in the melted state (to prevent sticking and premature crystallization by friction).

For demonstrations of on-demand shape-fixing, 2 mL of P10L10 (for the low-polymer case) or P30L10 (for the high-polymer case) was used. The gel samples were shaped and then touched with salt while held in shape to freeze *in-situ*.

For demonstrations of stability of sal-gel, 8 mL of P10L10 was used. The sal-gel was crystallized with a touch of salt, then coated in vacuum grease (silicone high vacuum grease; Dow Corning) in the frozen state (to easily apply a thick coating). The coated sal-gel was placed in a small plastic bag and fully melted (at 90°C for 30 minutes), then allowed to cool to room temperature. The bag containing the gel was impacted against a hard surface multiple times, then left for 30 minutes. The gel (which had not crystallized) was squeezed to show softness, then the gel was touched with a salt crystal. Crystallization was allowed to proceed over 30 minutes, after which the gel was squeezed again to show its hardness.

For demonstrations of soft-to-hard transitional contact, 1.5 mL of P10L10 was used. The sal-gel was brought into contact with a golf ball while in the melted state. In both melted and frozen cases, the gel was then lifted upwards by hand. However, for the frozen case, the gel was first crystallized by the touch of salt while in contact with the golf ball and left to freeze for 30 minutes in a closed environment.

For demonstrations of instant and robust self-adhesion, 2 mL of P10L10 was used to wrap around the bottlecap, and 3 mL of P10L10 was used for the handle. The first gel sample was wrapped around the top of a 1.5 L water bottle, then touched by salt and left for 10 minutes to freeze. While the bottle was held upside-down, the second sample was brought into contact and gently pressed onto the side of the first gel sample. Then, the other end of the second gel sample was brought around and briefly pressed into the other side of the frozen gel, to form a handle on the top of the water bottle. These gels were left to fully freeze overnight in a closed environment. Afterwards, the handle made from these two gel samples was used to lift up the 1.5 L bottle.

For demonstrations of on-demand mechanical energy storage, 8 mL of P10L10 was used. The sal-gel was coated in vacuum grease (to prevent evaporation and early crystallization by friction) and placed between two glass slides. The gel was then compressed to a thickness of 3 mm and crystallized with a touch of salt while under compression. Afterwards, the force was withdrawn from the gel, and a 50 g weight was placed on top. A heat gun (1740 Watts; Master Appliance) was then used to melt the gel, causing it to expand back to a thickness of 9 mm while carrying the 50 g weight. Finally, the weight was removed, at which point the gel returned to its original 10 mm thickness.

For demonstrations of smart construct for dynamic structure/mechanics, polydimethylsiloxane silicone (Sylgard 184; Dow Corning) was prepared by mixing resin and curing agent at a weight ratio of 10:1 and pouring 2 mL of this mixture onto a microscope glass slide (1 × 3"; VWR). Once the mixture had spread and self-leveled by surface tension, it was cured at 90°C for 90 minutes. To promote adhesion between the silicone and sal-gel, the surface of the flat side of the silicone was chemically modified by polymerizing acrylamide (>99%; Sigma-Aldrich). 2 mL of aqueous solution containing 0.2 g of acrylamide and 0.002 g of 2,2-diethoxyacetophenone was poured into the Teflon mold placed on the silicone, then cured *in-situ* by exposure to ultraviolet light. Afterwards, the polymerized solution was rinsed and rubbed off, leaving behind a modified surface with a white appearance. 0.5 mL of P10L10 was formed on this surface using the Teflon mold. For the demonstration, the silicone rubber was stretched to a strain of 10%, then the gel was touched with salt and left to freeze for 30 minutes, with the strain still applied. This strain was then released. Finally, the gel was heated with the heat gun to melt it. The gel was then cooled to room temperature, and this process was repeated once more with the same piece of rubber and gel to check reusability.

3D doodling of 'sea pickle' (Fig. 3.8)

Gel solutions of P10L10 were kept in syringes at 90°C and delivered with a 30-gauge needle under room conditions. The solution was cured *in-situ* using a hand-held ultraviolet light (365 nm UV-LED, FUWO;

Bangwo). Multiple syringes were used over the fabrication process of the 'sea pickle' (to ensure the solution was always heated before curing).

Preparation and demonstration of sug-gel (Fig. 3.8)

Sugar alcohol solution was prepared by heating xylitol ($\geq$99%; Sigma-Aldrich) at 120°C for at least 72 hours (to fully melt all crystallites). Polymer precursors were prepared by mixing acrylic acid (low water content, with 200 ppm 4-methoxyphenol as inhibitor, 99.5%; Alfa Aesar) monomer, N,N'-methylenebis(acrylamide) (99%; Sigma-Aldrich) crosslinker, and 4-methoxyphenol (99%; Sigma-Aldrich) inhibitor at a weight ratio of 100:5:10.

Sug-gel was prepared by mixing the sugar alcohol solution and the polymer precursors at 120°C at a weight ratio of 100:10 between the sugar alcohol and the monomer. Once the resulting mixture was homogeneous, 2,2-diethoxyacetophenone (>95%; Sigma-Aldrich) initiator was added to the mixture at a weight ratio of 1:100 relative to the monomer. The final mixture was centrifuged at 4000 rpm for 2 minutes to remove bubbles, was kept at 120°C for an additional 10 minutes to stabilize, and then cured by irradiating with an ultraviolet light source (365 nm, LED floodlight BigBeam; Labino) at a 10 cm distance for 5 min under room conditions. Samples were then cooled to room temperature (approximately 21°C) before use.

Mechanical properties of sug-gel were measured using indentation (as for sal-gel). Since sug-gel crystallizes significantly slower than sal-gel, to ensure complete freezing, the samples were given 1 month to freeze (after nucleation by touching with xylitol crystals) at room conditions.

To create the sug-gel gummy bear, sug-gel solution at 120°C was poured into a custom mold and then cured *in-situ*. The mold was fabricated using a gummy bear as the template and polydimethylsiloxane silicone (Sylgard 184; Dow Corning) as the molding material. To test evaporation, a sug-gel gummy bear

was placed in an open environment at 120°C for 1 week. Images of the gummy bear were taken after fabrication, crystallization, evaporation, and recrystallization.

3.4 Material transition and on-demand shape-fixing

Sal-gel was prepared by mixing melted sodium acetate trihydrate, $CH_3COO^-Na^+\cdot3H_2O$, with polymer precursors of poly(acrylic acid) (where the weight percentage of the monomers relative to the salt is denoted as P#) and a liquid mixture of acetic acid and water (where the weight percentage of the liquid relative to the salt is denoted as L#). The liquid mixture, with a formulation of $CH_3COOH\cdot3H_2O$, is the acid counterpart to the salt hydrate and is used to prevent the salt from forming anhydrous sodium acetate, which would lead to undesired phase separation. We observed that the resulting gel mixture remained transparent while melted before and after polymerization, suggesting the components involved are miscible with each other, which is consistent with our Flory-Huggins estimations (**Supplementary Note 3.1**).
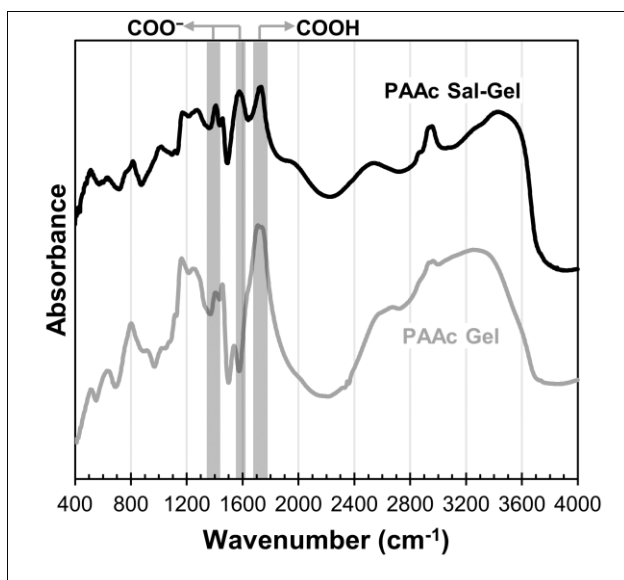
Fig. 3.2: Comparison between Fourier-transform infrared spectra for poly(acrylic acid) gel formed in sal-gel and formed in pure water.

The polymer precursors have a weight ratio of 100:1:1 between the monomers, crosslinkers, and initiators, respectively. While these samples showed a significant change in stiffness (from 8.9 ± 1.6 kPa to 83 ± 26 MPa for P10L10 in **Fig. 3.1a,b**), they had undesirably high sample variance. For this reason, we used a ratio of 100:5:1 for systematic studies, as the higher-crosslinker samples demonstrated better homogeneity in

the frozen state (with about 1/10 of the standard deviation compared to the lower-crosslinker samples).

After all the components were well-mixed and heated to 90°C, the polymer network was formed by exposure to ultraviolet light (365 nm) for 5 minutes (see **Methodology**). Using Fourier-transform infrared spectroscopy, we found that the chemical structure of the resulting network did not strongly differ from the same polymer network formed in pure water, displaying only a greater proportion of carboxylate groups to carboxylic acid, which is expected with the higher concentration of sodium ions in the system (**Fig. 3.2**). The resulting gel has two solid states: a transparent soft state that is easily deformable, and an opaque rigid state that resists deformation.

We can transform the sal-gel from its soft state to the rigid state by secondary nucleation *via* the touch of sodium acetate trihydrate seed crystals (**Fig. 3.1a**). Once in contact with a seed crystal (which could be as small as nanometers in scale[67]), nucleation occurs almost instantaneously (<< 1 sec) and crystallization (freezing) proceeds from the point of contact throughout the entire material. In all our experiments, we used a wooden stick with a small amount of fine crystal dust on the tip as the applicator to carry out the initiation. In addition to seed crystals, we noted that for samples that were soft and sticky, direct contact with sal-gel could trigger crystallization. Since this phenomenon seemed to only originate from samples' surface, we suspected that the cause is twofold: firstly, the free energy cost for nucleation is greatly lowered at the gel's surface due to reduction in the surface area of the nucleus; secondly, upon contact, the surface can experience an enormous amount of kinetic energy at points, with this localized friction leading to tribonucleation[66]. We found that so long as the gel remained slippery during handling, unintended crystallization never occurred. As such, we usually lubricate the surface (*e.g.* with a very small amount of water or oil) of sal-gel in the soft state; coating the gel with a thin layer of lubricant can extend this protection for the long term without interfering with its practical use. An additional benefit of lubrication is that it makes the gel easier to handle (as the gel is less sticky). We can revert the sal-gel to its soft state by heating it above the salt's melting point (>58°C); the sal-gel will retain this state, even

when cooled back to room temperature. Utilizing these properties, we can fix the shape of the gel on-demand (at any point in time) by deforming in the soft state and then inducing freezing by secondary nucleation (**Fig. 3.1b**). In addition, we can tune the physical properties of the frozen state by manipulating the polymer content of the gel. With low polymer content, the frozen gel is rigid and inflexible, and tends to fracture under deformation; with high polymer content, the frozen gel is elastic and flexible, such that it can withstand deformation, and will return to its fixed shape once the stress is released (**Fig. 3.1c**).

3.5 Contrast in mechanical behaviors and stiffness

We characterized the mechanical behavior of the two states of the sal-gel system under the same environment by indentation. In these tests, we performed each indentation twice at the same location, and to the same depth, immediately one after the other. **Fig. 3.3a-c** shows the typical material behavior for melted (**a**) and frozen sal-gel (**b**), as well as for the frozen salt without polymer (**c**). Comparing the melted and frozen sal-gel, the frozen gel displayed plastic deformation, with a large difference between the force-displacement curves for the first and second indents. In contrast, the melted sal-gel exhibited elastic behavior, where all loading and unloading curves closely overlapped with each other. While the plastic deformation of the frozen gel left a visible depression, this depression disappeared after melting. This suggests that the plastic deformation was stored by the solid salt crystal structures. The changes in plastic/elastic behavior were accompanied by a magnitudinal change in the force detected at the same indentation depth (45.7 N *vs.* 0.026 N). This suggests a significant change in stiffness between the two states. The frozen sal-gel was less brittle than the frozen polymer-free salt, allowing the material to reach a higher indentation force without cracking.

To further verify this mechanical behaviors of sal-gel, tensile measurements have been performed on P10L10. As shown in **Fig. 3.4**, while the gel in the frozen state is significantly stiffer than in the melted state, the plateau in its stress-strain curve suggests that the frozen gel is not brittle. Samples of pure salt (L10) were also made but were too fragile to be tested (*i.e.* they could not be removed from their molds intact). This further supports the reinforcing behavior of the polymer network in sal-gel observed from indentation testing. All samples of melted sal-gel failed early at their ends due to gripping. This demonstrates a synergy between the sal-gel's components, likely due to reinforcement of the salt crystals, or disruption of crack propagation, by the polymer network.
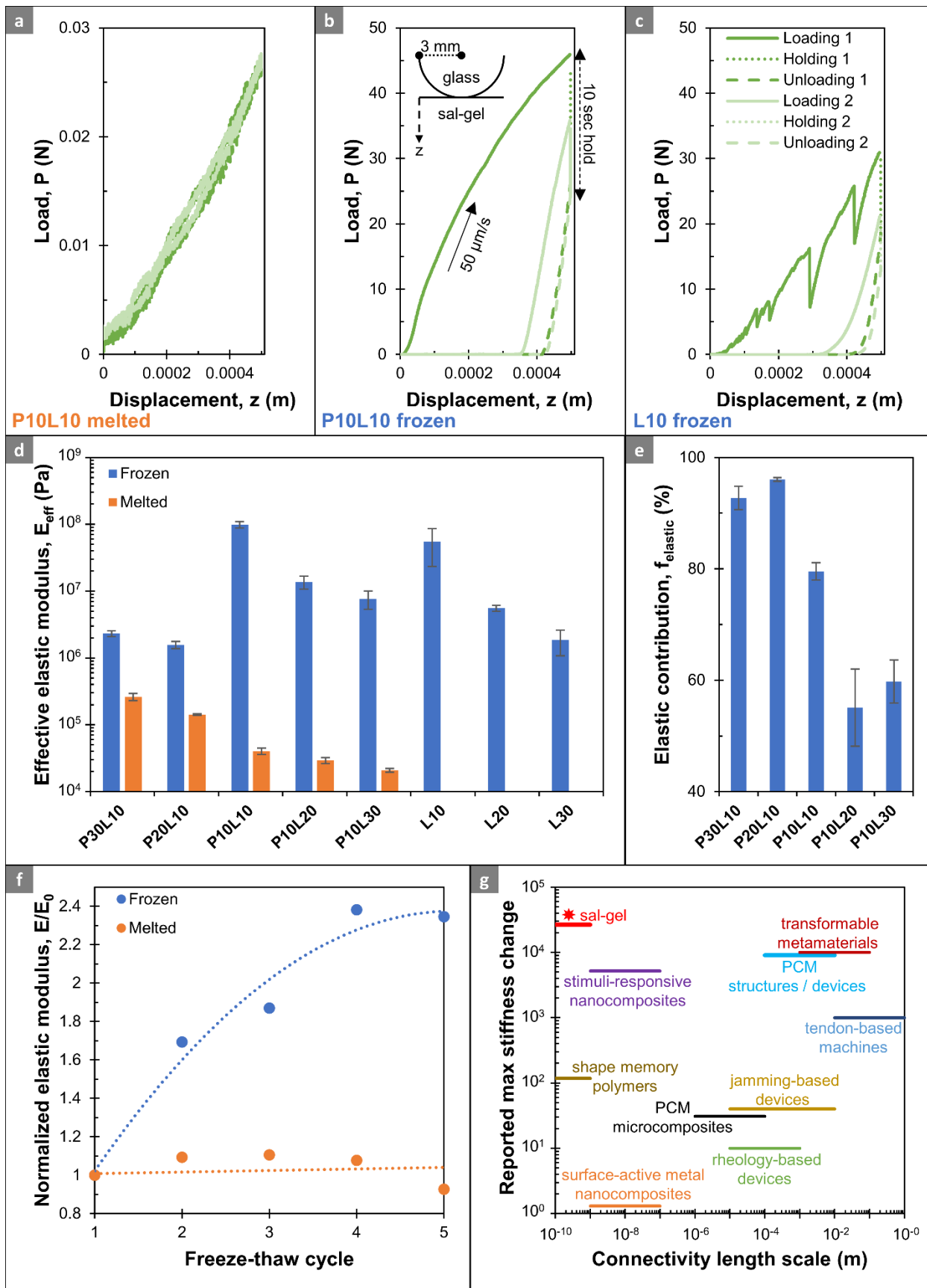
Fig. 3.3: Mechanical behaviors of sal-gel. a-c, Typical load-displacement curves for P10L10 melted (a), P10L10 frozen (b), and L10 frozen (c) samples in indentation tests. **d,e**, Mechanical characterization of sal-gel of different compositions with effective elastic moduli extracted from the initial loading curves (**d**) and elastic contributions of material response in the frozen state (**e**). **f**, A plot of relative change in elastic modulus for a P10L10 sample over 5 freeze-thaw cycles. **g**, The change in stiffness of sal-gel compared with other stiffness-changing materials/devices with respect to the length scale of connectivity. These (with their respective key references) include shape memory polymers[55,57], stimuli-responsive nanocomposites[53,54], surface-active metal nanocomposites[58], phase-change material (PCM) microcomposites[56], transformable metamaterials[59–61], rheology-based devices[77,78], jamming-based devices[79,80], PCM structures/devices[71–73], and tendon-based machines[81,82]. The error bars represent one standard deviation ($n \geq 3$).

P10L10 frozen

P10L10 melted
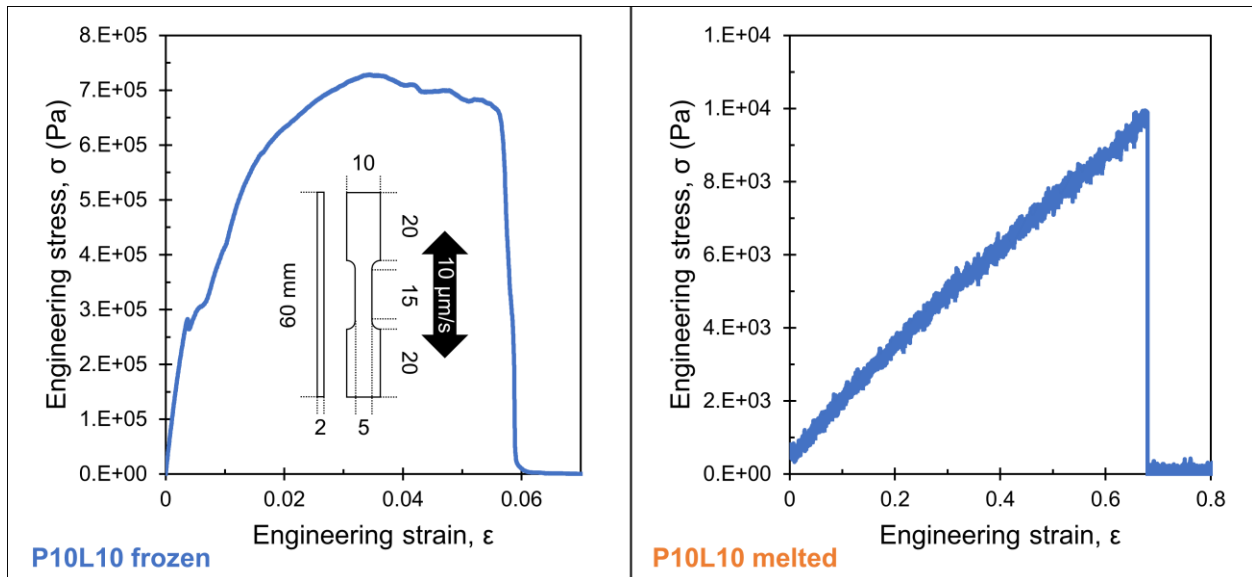
Fig. 3.4: Typical engineering stress *vs.* strain curves of sal-gel.

We extracted effective elastic moduli from the loading curves of the indentation tests by fitting the data with Hertzian contact mechanics (**Supplementary Note 3.3**). To further characterize any changes in mechanical behavior, we compared the first and second indents directly. We noted that their unloading

curves were nearly identical, suggesting all irreversible plastic deformation occurred during the first indent, so any force felt during the second indent should be due to the elastic/viscoelastic response. Hence, we estimated the elastic contribution to the material response by taking the ratio of the maximum indentation force of the second indent to the first. **Fig. 3.3d,e** displays the resulting moduli (**d**) and elastic contributions (**e**). We found that while low polymer fractions can reinforce the frozen sal-gel, high polymer fractions had the opposite effect, making the frozen gel softer and more elastic. However, this softness did not exclude the shape-fixing ability of the gel (**Fig. 3.3c**). In contrast to frozen gel's behavior, high polymer fractions led to stiffer melted sal-gels, which is expected, since the melted state behaves as a pure gel. With more acetic acid liquid mixture present, the sal-gel became softer and less elastic, as expected from the decrease in solid fraction. To understand if there was any lasting damage from indentation or from the freeze-thaw process, we repeatedly froze and thawed the gel, with one hour of freezing or thawing time each cycle, performing indentations at the same location after each freeze or thaw step (**Fig. 3.3f**). We did not observe a noticeable trend for the melted state of sal-gel, suggesting there was no lasting damage to the polymer network, while surprisingly, we found that the frozen gel became stiffer over repeated freeze-thaw cycles. Following the observed trends from indentation on different compositions, by further reducing both the polymer and liquid fractions, we obtained more than 10^4 times change in stiffness (P5L5; from 14.6 ± 1.6 kPa to 385 ± 32 MPa). This number was placed into perspective with respect to current technologies in **Fig. 3.3g**.

3.6 Crystallization behaviors

To interpret the indentation results and understand the underlying mechanisms, we investigated the crystallization process within the sal-gel from structural, kinetic, and thermal perspectives. **Fig. 3.5a** shows the growth of crystals in P10L10, progressing from pre-nucleation through to complete crystallization and back to the melted state. Secondary nucleation was initiated at a single point, leading to crystal growth through the gel network and the eventual crystallization of the entire gel, as seen in optical microscope images. The extent of crystallization confirmed that the underlying salt network was continuous. After subsequent melting, this crystal growth appeared to have left various micron-sized voids in the gel, which eventually disappeared with further heating (*e.g.* overnight), returning the gel to its original state. This suggests the growth of crystals had only pushed aside the polymer chains, rather than rupturing them, agreeing with the observation from the cycled indentation test that freezing does not damage the polymer network. Additionally, these voids indicate that the polymer chains obstructed the growth of the salt crystals. This is reinforced by observations that samples with higher polymer density had visibly smaller crystals, showing no observable voids upon melting. Coupled with the observation that more voids appeared with repeated freeze-thaw cycles (without giving enough time for the voids to heal), this can explain the observed increase in stiffness of the frozen sal-gel; with each freezing step, the salt crystals pushed out the polymer chains further, leaving less obstruction of crystal growth for the next cycle, resulting in a stronger network of crystals.
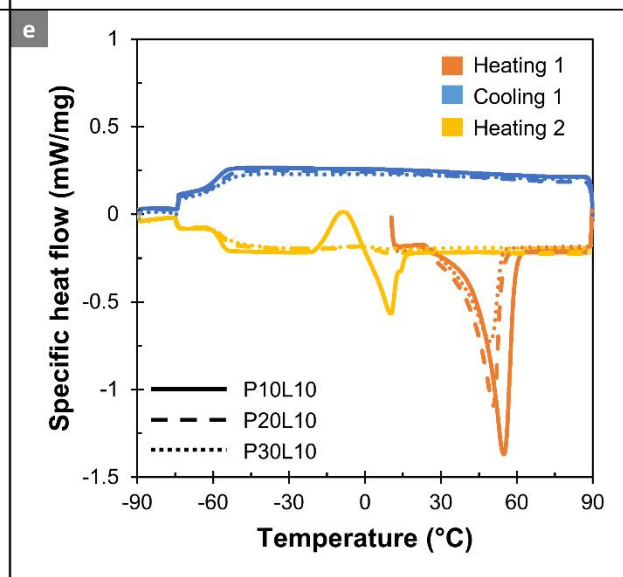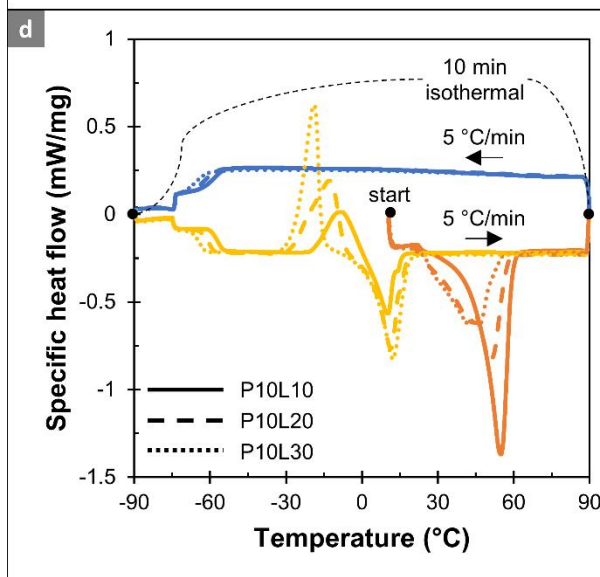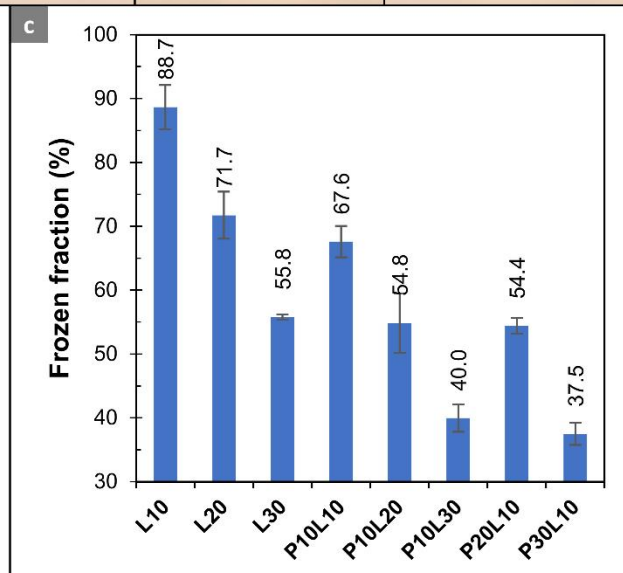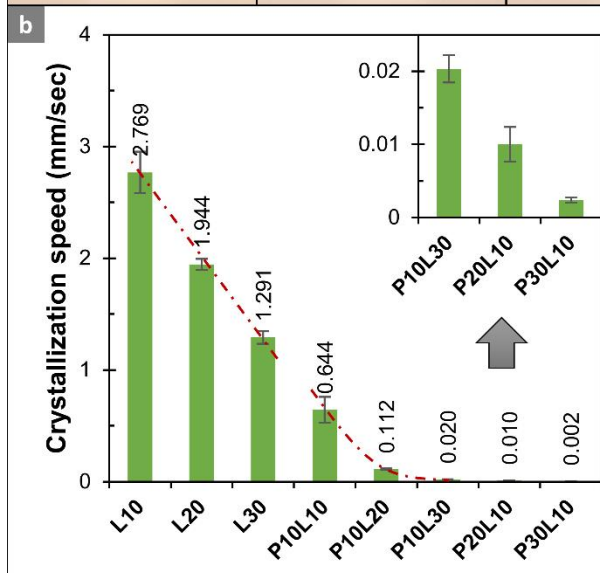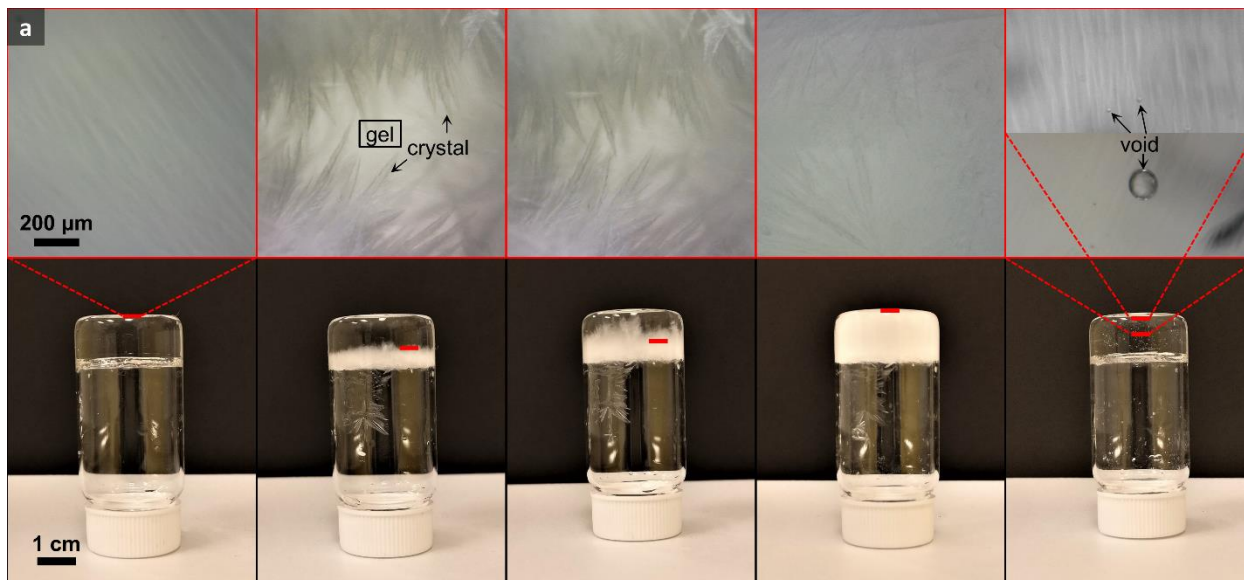
Fig. 3.5: Crystallization behaviors of sal-gel. a, Growth of salt crystals in sal-gel from a single nucleation point over time, with the crystals fully melted in the final images; the top and bottom rows of images show crystallization at the microscopic scale and the macroscopic scale, respectively; each microscopic image corresponds to the bottom macroscopic image on locations marked in red. **b**, A plot of crystallization speed for different samples; the red guidelines highlight the trends from L10 to L30 and from P10L10 to P10L30. **c**, A plot of the frozen fraction of salt for different samples. **d,e**, Typical specific heat flow *vs.* temperature curves from differential scanning calorimetry for different samples, which are plotted together with respect to varying acetic acid liquid mixture content (**d**) and varying polymer content (**e**). The error bars represent one standard deviation ($n \geq 3$).

To gain a kinetic perspective of crystal growth within the sal-gel, we initiated the crystallization of different samples from one end of a narrow tube and measured their one-dimensional growth rate. The results are shown in **Fig. 3.5b**. The rate appeared to be linear with respect to increasing fraction of liquid content for samples without polymer network, but exponential with respect to increasing fraction of either polymer or liquid content for samples with polymer network. These results can be explained by considering a simple kinetic model. Assuming that all collisions of salt molecules to existing crystals result in attachment, the rate, R, is proportional to the product of the diffusion coefficient, D, and the concentration, C, of free salt, $R \propto DC$. For the no-polymer case, D is expected to be similar across the samples, meaning that $R \propto C$, producing a linear trend with respect to the concentration change, which is approximately linear for L10, L20, and L30. On the other hand, the presence of polymer will significantly affect D. Most gel models show an exponential relationship between D and the polymer fraction, ϕ[83]. For instance, in the typical stretched exponential model for relating macromolecules' diffusion in polymer solution, $D \propto \exp(-a\phi^v)$, where a and v are experimentally fitted parameters[84]. Since changing either polymer or liquid content correspondingly changes ϕ, the observed exponential trend is expected. While the macroscopic trend can be explained by considering a simple model, the real situation is likely much more complicated. For

instance, since the size of salt crystals varies with polymer content, the respective surface areas of the crystals will be different, influencing the growth/nucleation rate, which is not covered by the simple rate model. In addition, the growth of crystals can be considered as a process of continuously generating new surfaces, where surface energy plays an essential role. It is well-known that the gel network influences the formation of crystals[85]. By constraining growth, it can induce a variety of crystal phases, each with a different surface energy. As a result, modeling of this material is likely very complicated, as one cannot generalize crystal growth behavior and kinetics.

To understand the thermal perspective of sal-gel crystallization, we performed a set of differential scanning calorimetry experiments, where we heated frozen samples to 90°C, then cooled them down to -90°C, then heated them back to 90°C. The phase-change behaviors of sal-gel samples are shown in **Fig. 3.5d,e** with respect to varying liquid (**d**) or polymer (**e**) contents. Compared to samples without polymer and to pure acetic acid liquid mixture (**Fig. 3.6**), we observed that the addition of polymer introduced multiphase melting behavior, visible in the broadening of the initial salt melting peaks with splitting for some of the cases (*e.g.* P10L20). We observed paired peaks for cold crystallization and melting upon reheating that increased with increasing liquid content, where the melting peaks occurred at much lower temperatures than those of the salt. As such, these peaks corresponded more to the acetic acid liquid mixture than the salt. In contrast, we observed no freezing peaks at higher polymer content, suggesting the polymer network affected the tendency of the liquid to freeze. Overall, the lack of salt crystallization peaks demonstrated a potential degree of supercooling of >150°C (which is one of the highest among all materials as far as we know), indicating strong stability of the sal-gel. We qualitatively verified this stability by applying high-force percussive impacts to (*i.e.* repeatedly and violently smacking) a piece of vacuum grease-coated unfrozen sal-gel (P10L10), which could not trigger crystallization, yet poking the gel with seed crystals still could. This outcome is reasonable considering that supercooled sodium acetate

trihydrate solution requires at least 200 bars of ambient pressure while under a sonicator capable of producing 475 W to initiate nucleation by shockwave[66].
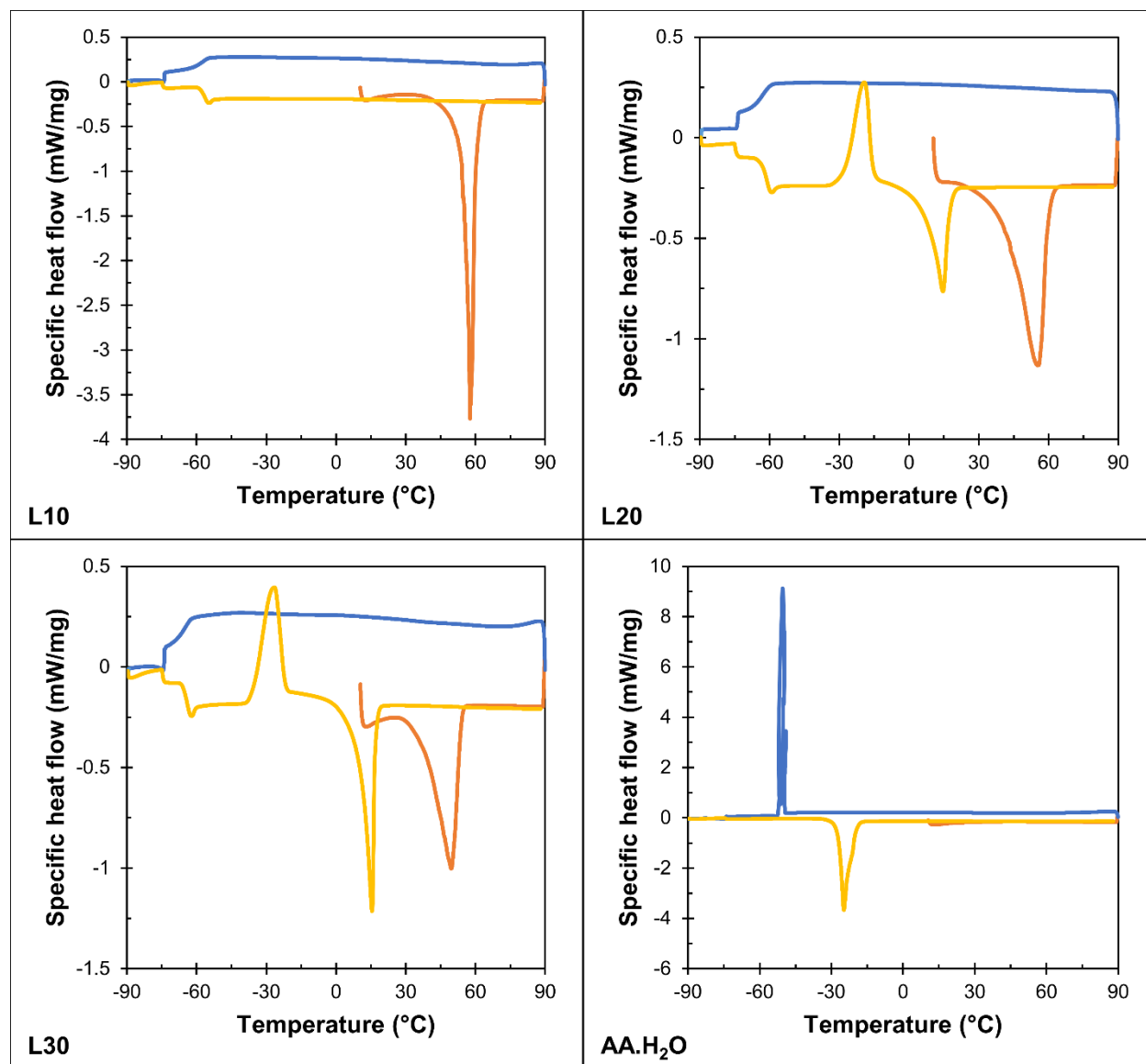
Fig. 3.6: Results from differential scanning calorimetry for L10, L20, L30, and pure acetic acid liquid mixture.

To elaborate on the extent of crystallization, we calculated the percentage of the salt that is frozen within a sal-gel by integrating its initial melting peak and comparing the result with the standard heat of fusion of the salt hydrate. The resulting frozen fractions are plotted in **Fig. 3.5c**, showing that increasing either

the polymer or liquid contents decreased the amount of frozen salt. These behaviors with respect to increasing liquid content can be explained by the corresponding decrease in the oversaturation of salt. For increasing polymer content, these behaviors can be explained by considering how water freezes in hydrogels. Water in hydrogels is known to be affected by specific interactions with polymer chains. Close to the chains, a portion of water is bound, resulting in greatly restricted mobility of the water molecules, which consequently do not freeze. Moving away from the chains, water is preferentially oriented around the bound water and the polymer network structure, such that they form a secondary or tertiary hydration shell due to the maximization of hydrogen bonds. This water does freeze, but at a lower temperature compared to unbound free water, which is further away from the chains[86]. We believe this situation would apply to the salt molecules as well, since they have strong interactions with the poly(acrylic acid), leading to non-freezable bound, less-freezable bound, and freezable free salt in sal-gel. This distribution of the forms of salt explains the broadening/splitting of the peaks and the reduction in frozen fraction with increasing polymer content.

In summary, the different perspectives from the investigation of the crystallization have come together to paint a coherent picture. In sal-gel, the polymer network obstructs the growth of crystals, resulting in slower growth, smaller crystals, and multiple crystal phases. Accordingly, more polymers lead to less freezing. This should contribute strongly to the behaviors we observed in indentation, since a less frozen gel would be less stiff. However, there are still details that cannot be fully resolved, such as the similarity in elasticity between P20L10 and P30L10, which have quite different frozen fractions. Some potential factors that could contribute to these details include narrower connections between crystals as they get smaller, the synergistic support of the crystals by the polymer network, and possible differences in elasticity associated with different phases of crystals. These complex behaviors indicate that the final properties of sal-gel are not simply additive of its components, suggesting these components interact with

each other at the molecular scale. This underlines that sal-gel is a new type of material, one that exhibits original capabilities for new applications.

3.7 Applications

In **Fig. 3.7**, we highlight four interesting applications of sal-gel: soft-to-hard transitional contact, instant and robust self-adhesion, mechanical energy storage, and the formation of smart constructs. For these demonstrations, depending on the volume of the material as well as the location and number of the initial nucleation sites, it typically took under 15 minutes for sal-gel to fix the shape formed from the soft state. For the first application, sal-gel's ability to switch between very soft and very rigid states allows it to conform and establish good contact with an object while soft, then become rigid enough to pick the object up and hold it firmly. This is illustrated using a golf ball in **Fig. 3.7a-d**. In this illustration, we lowered a piece of unfrozen sal-gel onto a golf ball (**a**), establishing contact by its own weight (**b**). If the sal-gel remained unfrozen, it was unable to pick up the golf ball (**c**); however, if it was instead frozen while in contact, it could pick up the ball and hold it (**d**). This behavior can be understood by considering the interface between the golf ball and sal-gel as a fracture. According to Griffith's criterion in fracture mechanics, the tensile stress, σ_f, required to propagate a fracture (*i.e.* to detach the gel from the golf ball) is described by $\sigma_f = \sqrt{\frac{EG}{\pi a}}$, where E is the elasticity associated with the materials near the fracture, a is the flaw length at the interface, and G is the interfacial adhesion. While in the soft state, the gel has a high G, but a very low E, making it easy to detach; however, through transitioning to a rigid state, the gel maintains the benefits of good contact (high G), while greatly increasing E, allowing maximal holding power.

a sal-gel (unfrozen)

b soft conformal contact

1 cm

c failure by peeling

d hard lasting bonding · sal-gel (frozen) · 46 g

contact · lift · soft-to-hard **transitional contact** · lift

e sal-gel (frozen) · sal-gel (unfrozen) · join

f instant & robust **self-adhesion** · lift

2 cm

g after fully frozen · ~ 1.5 kg

h sal-gel (unfrozen) · 10 mm

i W_{in} · 3 mm · press · freeze

j Q_{out} · sal-gel (frozen) · on-demand **mechanical energy storage** · +mass

2 cm

k 50 g · melt

l W_{out} · Q_{in} · −mass · 9 mm

m

n sal-gel (unfrozen) [t ≈ 0.5 mm] · PDMS [t ≈ 1 mm] · stretch · melt

o 10% strain · freeze

p sal-gel (frozen)

q >180° bending at rest · release

smart construct for dynamic structure/mechanics

2 cm

75

Fig. 3.7: Applications of sal-gel. a-d, A demonstration of the soft-to-hard transitional contact of sal-gel; a thin strip of unfrozen sal-gel (**a**, P10L10) is lowered into contact with a golf ball (**b**) and is then lifted off while the gel is unfrozen (**c**) or frozen (**d**). **e-g**, A demonstration of the instant and robust self-adhesion of sal-gel; a strip of unfrozen sal-gel (P10L10) is pressed against a frozen sal-gel (P10L10) which has been wrapped around a bottle cap (**e**); the unfrozen gel adheres on contact by freezing (**f**) and is able to lift up a bottle of water weighting around 1.5 kg after it is fully frozen (**g**). **h-m**, A demonstration of sal-gel as a mechanical energy storage; a very thick strip of unfrozen sal-gel (**h**, P10L10) is first compressed (**i**) and then frozen (**j**) to store mechanical energy; a weight is then added on top of the frozen gel (**k**); upon heating, the gel lifts the weight (**l**), producing work; upon removing the weight, the gel returns to its uncompressed original thickness (**m**). **n-q**, A demonstration of sal-gel for forming smart constructs; a very thin strip of unfrozen sal-gel (P10L10) is chemically bonded to a flat piece of silicone rubber (**n**); after stretching the rubber (**o**) and freezing the gel *in-situ* (**p**), the flat piece of rubber curves onto itself upon the release of external forces (**q**).

For the second application, we utilized the ability of sal-gel to establish instant and robust self-adhesion. In **Fig. 3.7e-g**, we illustrated this by joining one piece of unfrozen sal-gel to a frozen piece (**e**) to form a handle (**f**), which once fully frozen was then used to lift a water bottle weighing approximately 1.5 kg (**g**). The self-adhesion originates from the freezing of the supercooled salt of the unfrozen gel, initiated by secondary nucleation from contacting the salt crystals in the frozen gel and forming an instant and robust link between the salt crystals of the two gels. Since the gels were solely linked by salt crystals, they could be separated by melting the salt. This behavior may be suitable for assembly applications where instant and reversible bonding is required.

In the third application, we expanded on the capability of sal-gel for on-demand shape-fixing. Traditionally, sodium acetate trihydrate has been used for thermal energy storage[69]. However, by giving the melted salt

a solid form, we extended this material to function as on-demand mechanical energy storage. This is illustrated in **Fig. 3.7h-m**, wherein we took a thick piece of sal-gel (**h**), compressed (**i**) and then froze (**j**) it to store the mechanical energy from compression. Afterwards, we placed a weight on top of the compressed gel (**k**); the gel lifted the weight during melting, performing work (**l**). This gel returned to its original form once we removed the weight (**m**). In this process, the mechanical deformation of sal-gel would likely influence its crystal growth, as the gel network is intimately connected with the formation of salt crystals (according to the crystallization investigation). As a result, this extension of the salt to mechanical storage can not only lead to direct coupling of thermal and mechanical energy, but potentially enable a new form of conversion between the two.

In the last application, we exploited sal-gel's large change in stiffness, combining it with other materials to make a smart construct. We demonstrated an example of this in **Fig. 3.7n-q**, inducing bending of a strip of silicone rubber, which is a material commonly used in microelectromechanical systems and soft robotics. For this demonstration, we chemically bonded a very thin strip of unfrozen sal-gel to the rubber (**n**). Afterwards, we stretched the rubber to a strain of 10%, exerting around 5 N of force (**o**), and then froze the gel *in-situ* (**p**). When we stopped stretching, the frozen gel resisted deformation, causing the rubber to curl in on itself, resulting in a shape far different from its initial state (**q**). However, melting the gel returned the rubber to its original shape. Although the gel had cracked during curling due to the dramatic bending, this situation did not seem to greatly affect its usability, as we were able to reproduce this result with the cracks present by repeating the process. This example illustrates that sal-gel's stiffness switching can be used to control shape, which is useful for creating more advanced microelectromechanical devices. Alternatively, sal-gel could also be used to restrict the degrees of freedom of soft materials by locally increasing their stiffness. This feature mimics one of the major inspirations for soft robotics – the octopus, which stiffens its tentacles for accurate movements[87] – enabling soft machines to toggle between movements that are soft and adaptable or hard and precise.

3.8 Practical implications

One major advantage towards the application of sal-gel is that it is a self-contained single material that can be easily processed for additive manufacturing. To demonstrate this, we fabricated a 'sea pickle' (a sea cucumber made sour and salty by sal-gel) *via* 3D-doodling by delivering un-crosslinked sal-gel solution with a syringe and crosslinking the solution *in-situ* with a focused ultraviolet light source (**Fig. 3.8a-c**). The resulting print closely resembled a living sea cucumber in both appearance (**Fig. 3.8d-g**) and mechanics (**Fig. 3.8h,I**; where the dermis of sea cucumber can switch between a soft state for dexterity and a rigid state for protection[49]). In the soft state, the 'sea pickle' was transparent (with some whiteness visible due to lighting and voids in the sample as the rigid state was imaged first) and easy to depress by a finger (**h**). In the rigid state, the 'sea pickle' was opaque and thorny, pricking the finger upon depression (**i**).

a b c

d e f g

15
30 mm
8

h sal-gel (unfrozen) i sal-gel (frozen)

j xylitol ← sug-gel (unfrozen) k ← sug-gel (frozen) l m

5 mm

crystallize → evaporate at 120°C for 1 week → crystallize →

n

Frozen elastic modulus, E_{eff} (MPa) — Frozen
Melted elastic modulus, E_{eff} (kPa) — Melted

Temperature (°C)

o

Typical solid

		solid states
linear path	S1	
C1	P1	
C2	P2	
C3	P3	
C4	P4	
C5	P5	
C6	P6	

environmental conditions | material properties

Two-in-one solid

|		
nonlinear path	S1	S2
C1	P1	P2
C2	P3	P4
C3	P5	P6
C4	P7	P8
C5	P9	P10
C6	P11	P12

79

Fig. 3.8: Practical implications of sal-gel. a-c, A demonstration of the processability of sal-gel for additive manufacturing by fabricating a 'sea pickle' *via* 3D-doodling, showing the fabrication at the beginning (**a**), middle (**b**, for making base), and final (**c**, for making spikes) stages. **d-g**, A demonstration of the completed synthetic 'sea pickle' in comparison to a living spiny sea cucumber (*Pentacta anceps*; **d**) with the 'sea-pickle' at different viewing angles (**e-g**). **h,i**, A demonstration of 'sea pickle' at two different solid states, transparent and easily depressed by a finger in the soft state (**h**) and opaque and able to prick the finger in the rigid state (**i**). **j-m**, A demonstration of a sug-gel gummy bear containing more than 90 wt.% of sugar alcohol liquid content, showing that the sug-gel has the same dual states behavior as sal-gel (**j,k**), is practically non-evaporative (**l**) and can still crystallize after prolonged overheating (**m**). **n,o**, The implication of having two solid states; the elastic modulus of sal-gel responds to temperature changes very differently for each state (**n**), showing that materials with two states (S1, S2) can follow a non-linear path with respect to environmental conditions (C1-C6) and material properties (P1-P12) (**o**). The error bars in the plot represent one standard deviation ($n \geq 3$).

The translation of sal-gel into practical applications requires the resolution of two technical issues. The first issue is evaporation, due to leveraging liquid properties in ambient conditions. For sal-gel, the evaporation of water would convert sodium acetate trihydrate into its anhydrous form, which has a melting point of 324°C, thus limiting its switchability. Coating sal-gel with vacuum grease can alleviate the problem of evaporation, but does not resolve this issue entirely. To demonstrate one possible solution to this problem and that the concept behind sal-gel can be extended to other materials, we applied the fabrication processes of sal-gel to xylitol, a sugar alcohol, as the phase-change material. Xylitol is capable of supercooling[88] and nearly non-evaporative ($P_{vapor} = 0.0113 \, mmHg$ as predicted by the EPISuite™ from the US Environmental Protection Agency), such that it can avoid drying out in any practical timescale. Compared with sodium acetate trihydrate, while xylitol crystallizes more slowly due to its high viscosity, it only has a single crystal form so that evaporation would not affect its switchability. Using this sugar

alcohol, we made a sug-gel (sugar-gel) gummy bear that contained greater than 90 wt.% of xylitol (**Fig. 3.8j-m**). We found that this gummy bear showed the same two solid states behavior as sal-gel under room conditions (**j,k**), with elastic moduli of 60.0 ± 2.3 kPa and 680 ± 74.4 MPa for the melted and frozen states, respectively. After overheating at 120°C to accelerate evaporation for a week, the gummy bear's volume did not visibly change (**k,l**). While the sug-gel darkened in color during this process (likely due to degradation of the xylitol), this change did not greatly affect its ability to freeze on-demand (**l,m**), with elastic moduli of 62.0 ± 7.1 kPa and 450 ± 141 MPa for melted and frozen states, respectively (in fact, we had samples stored at 120°C for over two months – loosely equivalent to 170 years at 20°C – with negligible loss of volume that still showed the behavior of dual states). The other issue is the sensitivity of melted sal-gel's surface to tribonucleation, which may limit its implementation into applications. While this issue can be partially addressed by coating the sal-gel with lubricant, further engineering sal-gel to increase its stability could fully resolve this limitation, as suggested by supercooled materials that are stable enough for commercial uses (*e.g.* sodium acetate heat packs).

Overall, sal-gel exemplifies the versatility of "two-in-one" solids (**Fig. 3.8n,o**). To elaborate, we measured and compared the effective elastic modulus of sal-gel at different temperatures (21, 30, 40, and 50°C for P10L10) for each state (**n**). The results showed that the two states responded to temperature oppositely, with different magnitudes of response. The elasticity of the soft state increased with increasing temperature, which might be attributed to rubber elasticity, where the retractive force depends more on entropy than on enthalpy, and scales positively with temperature[89]. On the other hand, the elasticity of the rigid state decreased with increasing temperature, which corresponds to the broad melting peak observed from differential scanning calorimetry, where the crystals in the gel do not melt simultaneously (**Fig. 3.5d,e**). This shows that sal-gel, with two solid states, can follow a non-linear path with respect to environmental conditions and material properties, giving it more flexibility in design and functionality than normal solids with a single solid state (**o**).

3.9 Concluding remarks

In this work, we strategically constructed a solid framework inside a functional liquid – supercooled melted salt (sodium acetate trihydrate) – *via* the formation of a compatible polymer network poly(acrylic acid), creating a hybrid material, sal-gel. The synergy from having the components interacting with each other at the molecular level allowed us to leverage the properties of the liquid, exploiting its phase transition and metastability. Consequently, sal-gel exhibited material behaviors that, to the best of our knowledge, are not found in nature: having two stable and reversible solid states that can each exist under the same conditions for a range of conditions, with multiple orders of magnitude difference in the mechanical properties for each state. This in turn established a new functional aspect, where stiffness states do not require stimulus to maintain, inspiring new capabilities for use in advanced applications. Although this work has focused on the transformation of supercooled liquid, our approach might be extended to other liquids of different functionalities, potentially enabling new materials with exciting applications.

3.10 Supplementary information

Supplementary notes

Supplementary Note 3.1: Calculation of free energy of mixing by Flory-Huggins theory

According to Flory-Huggins theory[90], the free energy of mixing (ΔG_{mix}) is related to enthalpy (ΔH_{mix}) and entropy (ΔS_{mix}) as:

$$\Delta G_{mix} = \Delta H_{mix} - T\Delta S_{mix} = [RT\chi_{12}\phi_1\phi_2] - T\left[-R\left(\frac{\phi_1}{n_1}\ln\phi_1 + \frac{\phi_2}{n_2}\ln\phi_2\right)\right] \qquad \text{S. Eq. 3.1}$$

$$\Delta G_{mix} = RT\phi_1\phi_2\left[\frac{\ln\phi_1}{n_1\phi_2} + \frac{\ln\phi_2}{n_2\phi_1} + \chi_{12}\right] \qquad \text{S. Eq. 3.2}$$

The formulae for enthalpy and entropy are derived from statistical thermodynamics for a mixture of components of 1 and 2 where R is the ideal gas constant, T is the absolute temperature, ϕ is the volume fraction, n is the number of sites occupied, and χ is the dimensionless Flory-Huggins binary interaction parameter. For $\Delta G_{mix} \leq 0$, $\frac{\ln\phi_1}{n_1\phi_2} + \frac{\ln\phi_2}{n_2\phi_1} + \chi_{12} \leq 0$. When $\chi_{12} \leq -\max\left[\frac{\ln\phi_1}{n_1\phi_2} + \frac{\ln\phi_2}{n_2\phi_1}\right]$, the components are miscible with each other at any mixture compositions. When component 1 and 2 are solvent and small monomer molecules, respectively, they each occupy one solvent site, so $n_1 = 1$ and $n_2 \approx 1$. Since $\max\left[\frac{\ln\phi_1}{n_1\phi_2} + \frac{\ln\phi_2}{n_2\phi_1}\right] = -4\ln 2 \approx -2.78$, the components are fully miscible when $\chi_{12} \leq 2.78$. When component 1 and 2 are solvent and polymer, respectively, $n_1 = 1$ and n_2 is the number of sites occupied by a polymer chain (the molar volume of the polymer divided by the molar volume of the solvent), which is typically a very large number, so that $\frac{\ln\phi_2}{n_2\phi_1} \approx 0$. Since $\max\left[\frac{\ln\phi_1}{n_1\phi_2} + \frac{\ln\phi_2}{n_2\phi_1}\right] = \max\left[\frac{\ln\phi_1}{n_1\phi_2}\right] = -1$, the components are fully miscible when $\chi_{12} \leq 1$.

For sal-gel, the Hansen Solubility Parameters (HSP) for poly(acrylic acid) and sodium acetate trihydrate, shown in Supplementary Table 1, have been estimated from the "HSP Excel Sheet" available from hansen-solubility.com where the interaction parameters for acrylic acid and different solvents have been taken from Hansen Solubility Parameters: A Users' Handbook[76].

Supplementary Table 1: Estimated Hansen solubility parameters for sal-gel components.

	Soluble In	Insoluble In	dD	dP	dH	MVol	R_0
Acrylic acid			17.7	6.4	14.9		
Polyacrylic acid	Water, Ethanol, Methanol, Glycerol, Acrylic Acid, Tetrahydrofuran	Acetone, Diethyl Ether, Hexane, Heptane	15.8	9.0	15.1		8.2
Sodium acetate trihydrate	Water, Ethanol, Methanol, Acetone, Ethylene Glycol, Formic Acid, Acetic Acid, Hydrazine, Dimethylforamide, Glycerol	Hexane, Benzene, Heptane, Toluene	16.5	11.3	18.2	93.86	11.4

Assuming the molar volume ($MVol$) is approximately that of sodium acetate trihydrate and $T = 363\ K$

and based on HSP distance (R_a) and its relation to χ_{12}[91]:

$$R_a^2 = 4(dD_1 - dD_2)^2 + (dP_1 - dP_2)^2 + (dH_1 - dH_2)^2 \qquad \textbf{S. Eq. 3.3}$$

$$\chi_{12} = \frac{MVol \cdot R_a^2}{RT} \qquad \textbf{S. Eq. 3.4}$$

$\chi_{12} = 0.317 \ll 2.78$ for acrylic acid in salt and $\chi_{12} = 0.131 \ll 1$ for poly(acrylic acid) in salt.

Supplementary Note 3.2: Rationale behind connectivity length scales

Devices/machines

Devices/machines are objects assembled with distinguishable parts of different materials. Consequently, for stiffness-switching devices, the parts responsible for changing stiffness define the connectivity length scale. For example, rheological based devices are typically composed of polymer microchannels filled with magnetorheological fluid. Shrinking the microchannels below 10 μm will pose major technical challenges, both for device fabrication and for introducing the fluid into the channel due to the surface tension of the fluid. Consequently, we estimated the connectivity length scale for rheology-based devices to range from 10 μm to mm.

Metamaterials

Metamaterials are objects composed of structural cells that can be transformed, for which the transformation is responsible for changing stiffness. When a structural cell scales below 100 μm, surface forces can pose substantial issues for transforming the cell (*e.g.* folding can become irreversible due to high interfacial adhesion). Considering the typical transformation requires multiple cells to work in unison, we estimated the connectivity length scale for transformable metamaterials to range from mm to 10 cm.

Micro/nanocomposites

Micro/nanocomposites are materials with micro- and nano-fillers, where the fillers are responsible for changing stiffness. Thus, we expected the connectivity length scale for these composites to be the same as the minimum length scale of the fillers, ranging from 1 nm to 100 nm for nanocomposites, and 1 μm to 100 μm for microcomposites.

Polymeric materials

Shape-memory polymers/sal-gel are materials with constituents interacting with each other at the molecular level. Accordingly, the change in stiffness for these materials also occurs at the molecular scale, resulting in a connectivity length scale that ranges from 1 Å to 1 nm.

Supplementary Note 3.3: Indentation data processing *via* Hertzian contact mechanics

For our indentation experiments, according to Hertz[92], the effective elastic modulus of sal-gel (E^*) is related to the radius of the glass probe (R), the load (P), and displacement (d) as:

$$E^* = \frac{3P}{4R^{1/2}d^{3/2}}$$

S. Eq. 3.5

The data point for each pair of P and d in the initial loading curve from indentation was converted to E^*. The average E^* from the loading data was reported, where the change in E^* with respect to displacement is shown in **Fig. 3.9**.
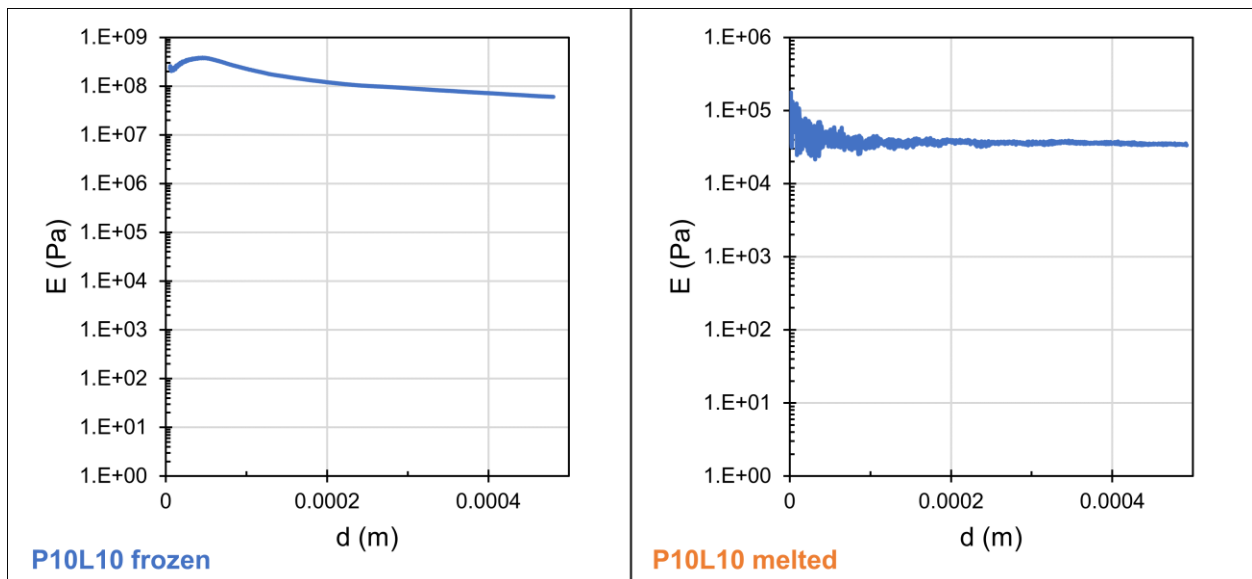

Fig. 3.9: Typical values for E* with respect to displacement.

Chapter 4. Conclusions and Future Work

In this thesis, we explored polymer gels as soft functional solids. Here in this section, we summarize key scientific contributions of this thesis and potential extended future works from the author's perspective.

4.1 Contribution of molecular conformation to interfacial adhesion

In the first work of this thesis, we investigate how the noncovalent interactions in gels (a gel coating) can be manipulated *via* molecular conformation to enhance the gels' adhesion with other materials. The key contribution of this work is the confirmation of a connection between molecular conformation at the molecular level and interfacial adhesion at the macroscopic level. Note that while there are several works on generating macroscopic adhesion *via* host-guest supramolecular chemistry, these works do not address this connection as they rely on modifying/creating materials with specific and complementary supramolecular structures rather than on the molecular conformation of the materials themselves. Despite prevalence of the technique of molecular imprinting, in which a material's molecular conformation is manipulated to enhance its affinity to specific small molecules, as well as the vast amount of evidence associated with localized adhesion (binding) of biomolecules as a result of molecular conformation (shape of biomolecules), this connection has only been speculated to date due to the difficulty associated with acquiring direct molecular details on conformation. In this work, we addressed this difficulty by performing a series of carefully designed and interconnected indirect experiments. We employed polydopamine, a nanoscale mussel-inspired gel coating, as a platform, wherein noncovalently interacting small guest molecules that resembled a particular hydrogel were added and then removed during the formation of the coating to affect the coating's conformation. We then examined the adhesion between the resulting gel coating and the respective hydrogel, which was formed *in-situ* on the coating. To ensure the experimental results were representative, we tested three different classes of hydrogels (*i.e.* ionic, chemically, and physically crosslinked), where the associated guest molecules have different interactive strengths (ranging from strong coordination bonds to van der Waals) with polydopamine. We

also examined three different types of materials (*i.e.* metal, plastic, and ceramic) for the underlying substrate of the coating, as the nanoscale thickness of the coating means that influence of the substrate cannot be ignored. To prove the measured macroscopic adhesion between the hydrogels and the coating could be traced back to the molecular conformation of the coating we measured the interactions between the coating and the hydrogels at various length scales. These length scales ranged from molecular, microscopic, to macroscopic, and interactions were investigated using a variety of techniques including quartz crystal microbalance, computer modeling, micro-indentation, and tensile tests. The associated results demonstrated reasonably correlated increase in interactions due to conformational changes consistently over different length scales and different experimental conditions, showing that the conformational changes at an interface can lead to up to a 2-3 fold increase in macroscopic adhesion. Forthermore, we demonstrated that coupling this increase in adhesion with energy dissipation could be applied for the bonding of materials.

4.2 Future work on molecular conformation

The outcome of this work implies that the molecular conformation at an interface has a significant effect on the interfacial interactions at the macroscopic level, suggesting that techniques such as molecular imprinting could be used to affect the adhesion/recognition of materials at larger length scales. To this end, we believe it is worthwhile in the future to develop a theoretical framework correlating conformation with adhesion (which we could not do so in this work due to the lack of experimental resolution and the physical limitations associated with the existing analytical techniques for conducting experiments in wet conditions).

4.3 Contribution of supercooled liquid to the material properties of gels

In the second work of this thesis, we leveraged the unique material nature of gels. The fundamental difference between gels and other soft pure solids (*e.g.* natural rubber and PDMS) is that gels contain liquid. Conceptually, this difference means that gels should be able to achieve functional properties that are not attainable by pure solids. In this work, we demonstrated this notion by converting a supercooled liquid into a gel. Due to the liquid having a supercooled metastable liquid state and a crystallized stable solid state, the resulting gel has two reversible and stable solid states with a stiffness change between the two of up to 10^4 times. These material properties are only achievable due to the liquid aspect of gels. While polymers in pure solids such as natural rubber can also supercool, it is nearly impossible for these solids to attain two reversible and stable solid states because their states would be disrupted by material deformations, which affect the alignments of polymers. On the other hand, this is not an issue for gels because of the mobility of the liquid, making its microscopic order almost independent of macroscopic material deformations. Moreover, the large transformation in stiffness is a result of the phase transition of the liquid from liquid to solid, which has a much larger change in molecular connectivity than it would if both states are solid.

4.4 Future work on gels as functional materials

While we have successfully demonstrated that gels can have properties that far outperform pure solids, for these materials to be truly considered functional solids, one should be able to interact with gels as if they are pure solid materials. This requirement means that gels should be stable in air and in their interactions with other matters (liquid and/or solid depending on the intended application). The stability in air can be easily met by using a liquid that is non-evaporative, which we have done in this work. However, the stability in interactions is much trickier to attain. For example, when a gel is in contact with a porous solid, the leaching of liquid from the gel to the solid is almost inevitable due to surface tension and capillary actions. Consequently, there is a need of a solution to control the transfer of liquid in gels. One

potential solution might be coating the gels with a layer to prevent or control their contact with other materials. However, this solution is rather inelegant; a better solution might be for the gel to autonomously generate the surface layer, so that even if the gel is cut in half, the new surfaces of the gel would also be protected. As such, we believe that controlling the surface properties of gels *via* self-assembly or other autonomous processes would extend the practical usage of these functional gels and is a research topic worth exploring in future.

References

1.   *Physics of Polymer Gels*. *Physics of Polymer Gels* (Wiley, 2020). doi:10.1002/9783527346547.

2.   Hassan, P. A., Verma, G. & Ganguly, R. *Soft materials-properties and applications*. *Functional Materials* (Elsevier Inc., 2012). doi:10.1016/B978-0-12-385142-0.00001-5.

3.   Yang, C. & Suo, Z. Hydrogel ionotronics. *Nat. Rev. Mater.* **3**, 125–142 (2018).

4.   Hoare, T. R. & Kohane, D. S. Hydrogels in drug delivery: Progress and challenges. *Polymer (Guildf).* **49**, 1993–2007 (2008).

5.   Terech, P. & Weiss, R. G. Low molecular mass gelators of organic liquids and the properties of their gels. *Chem. Rev.* **97**, 3133–3159 (1997).

6.   Chen, Q., Chen, H., Zhu, L. & Zheng, J. Fundamentals of double network hydrogels. *J. Mater. Chem. B* **3**, 3654–3676 (2015).

7.   Gong, J. P., Katsuyama, Y., Kurokawa, T. & Osada, Y. Double-Network Hydrogels with Extremely High Mechanical Strength. *Adv. Mater.* **15**, 1155–1158 (2003).

8.   Sun, J.-Y. *et al.* Highly stretchable and tough hydrogels. *Nature* **489**, 133–6 (2012).

9.   Holten-Andersen, N. *et al.* pH-induced metal-ligand cross-links inspired by mussel yield self-healing polymer networks with near-covalent elastic moduli. *Proc. Natl. Acad. Sci. U. S. A.* **5**, 3–7 (2011).

10.   Berg, J. M., Tymoczko, J. L. & Stryer, L. Chemical Bonds in Biochemistry. in *Biochemistry* (W. H. Freeman, 2002).

11.   Hatakeyama, H. & Hatakeyama, T. Interaction between water and hydrophilic polymers. *Thermochim. Acta* **308**, 3–22 (1998).

12.   Dimitriyev, M. S., Chang, Y. W., Goldbart, P. M. & Fernández-Nieves, A. Swelling thermodynamics

and phase transitions of polymer gels. *Nano Futur.* **3**, 1–43 (2019).

13. Eslami, H. & MÜller-Plathe, F. Solvation In Polymers. in *Climate Change 2013 - The Physical Science Basis* (ed. Canuto, S.) vol. 6 279–320 (Springer Netherlands, 2008).

14. Wolfe, J., Bryant, G. & Koster, K. L. What is 'unfreezable water', how unfreezable is it and how much is there? *Cryo-Letters* **23**, 157–166 (2002).

15. Southall, N. T., Dill, K. A. & Haymet, A. D. J. A view of the hydrophobic effect. *J. Phys. Chem. B* **106**, 521–533 (2002).

16. Levy, Y. & Onuchic, J. N. Water Mediation in Protein Folding and Molecular Recognition. *Annu. Rev. Biophys. Biomol. Struct.* **35**, 389–415 (2006).

17. Mansoori, G. A. & Rice, S. A. Confined Fluids: Structure, Properties and Phase Behavior. *Adv. Chem. Phys.* **156**, 197–294 (2014).

18. Granick, S. Motions and relaxations of confined liquids. *Science (80-.).* **253**, 1374–1379 (1991).

19. Venkatram, S., Kim, C., Chandrasekaran, A. & Ramprasad, R. Critical Assessment of the Hildebrand and Hansen Solubility Parameters for Polymers. *J. Chem. Inf. Model.* (2019) doi:10.1021/acs.jcim.9b00656.

20. Shi, Q. *et al.* Bioactuators based on stimulus-responsive hydrogels and their emerging biomedical applications. *NPG Asia Mater.* **11**, (2019).

21. Talebian, S. *et al.* Self-Healing Hydrogels: The Next Paradigm Shift in Tissue Engineering? *Adv. Sci.* **6**, (2019).

22. Qiao, Z., Parks, J., Choi, P. & Ji, H. F. Applications of highly stretchable and tough hydrogels. *Polymers (Basel).* **11**, (2019).

23. Chivers, P. R. A. & Smith, D. K. Shaping and structuring supramolecular gels. *Nat. Rev. Mater.* **4**, 463–478 (2019).

24. Zhang, W. *et al.* Catechol-functionalized hydrogels: biomimetic design, adhesion mechanism, and biomedical applications. *Chem. Soc. Rev.* **49**, 433–464 (2020).

25. Zhang, P., Zhao, C., Zhao, T., Liu, M. & Jiang, L. Recent Advances in Bioinspired Gel Surfaces with Superwettability and Special Adhesion. *Adv. Sci.* **6**, (2019).

26. Alberts, B. *et al.* Proteins. in *Molecular Biology of the Cell* (eds. Wilson, J. & Hunt, T.) 109–172 (Garland Science, 2017). doi:10.1201/9781315735368-3.

27. Hartwig, A. *et al.* Mutual Influence Between Adhesion and Molecular Conformation: Molecular Geometry is a Key Issue in Interphase Formation. *J. Adhes.* **89**, 77–95 (2012).

28. Sharpe, L. H. The Interphase in Adhesion. *J. Adhes.* **4**, 51–64 (1972).

29. Sharpe, L. H. Some Thoughts About the Mechanical Response of Composites. *J. Adhes.* **6**, 15–21 (1974).

30. Saiz-Poseu, J., Mancebo-Aracil, J., Nador, F., Busqué, F. & Ruiz-Molina, D. The Chemistry behind Catechol-Based Adhesion. *Angew. Chemie - Int. Ed.* **58**, 696–714 (2019).

31. Lee, H., Scherer, N. F. & Messersmith, P. B. Single-molecule mechanics of mussel adhesion. *Proc. Natl. Acad. Sci. U. S. A.* **103**, 12999–3003 (2006).

32. Maier, G. P., Rapp, M. V., Waite, J. H., Israelachvili, J. N. & Butler, A. Adaptive synergy between catechol and lysine promotes wet adhesion by surface salt displacement. *Science* **349**, 628–32 (2015).

33. Lee, H., Dellatore, S. M., Miller, W. M. & Messersmith, P. B. Mussel-inspired surface chemistry for

multifunctional coatings. *Science* **318**, 426–30 (2007).

34. Alfieri, M. L. *et al.* Structural Basis of Polydopamine Film Formation: Probing 5,6-Dihydroxyindole-Based Eumelanin Type Units and the Porphyrin Issue. *ACS Appl. Mater. Interfaces* **10**, 7670–7680 (2018).

35. Dreyer, D. R., Miller, D. J., Freeman, B. D., Paul, D. R. & Bielawski, C. W. Elucidating the structure of poly(dopamine). *Langmuir* **28**, 6428–35 (2012).

36. Hong, S. *et al.* Non-covalent self-assembly and covalent polymerization co-contribute to polydopamine formation. *Adv. Funct. Mater.* **22**, 4711–4717 (2012).

37. Liebscher, J. *et al.* Structure of polydopamine: a never-ending story? *Langmuir* **29**, 10539–48 (2013).

38. Della Vecchia, N. F. *et al.* Building-Block Diversity in Polydopamine Underpins a Multifunctional Eumelanin-Type Platform Tunable Through a Quinone Control Point. *Adv. Funct. Mater.* **23**, 1331–1340 (2013).

39. Delparastan, P., Malollari, K. G., Lee, H. & Messersmith, P. B. Direct Evidence for the Polymeric Nature of Polydopamine. *Angew. Chemie* **131**, 1089–1094 (2019).

40. Palladino, P., Bettazzi, F. & Scarano, S. Polydopamine: surface coating, molecular imprinting, and electrochemistry—successful applications and future perspectives in (bio)analysis. *Anal. Bioanal. Chem.* **411**, 4327–4338 (2019).

41. Ball, V., Frari, D. Del, Toniazzo, V. & Ruch, D. Kinetics of polydopamine film deposition as a function of pH and dopamine concentration: Insights in the polydopamine deposition mechanism. *J. Colloid Interface Sci.* **386**, 366–372 (2012).

42. Harrington, M. J., Masic, A., Holten-Andersen, N., Waite, J. H. & Fratzl, P. Iron-clad fibers: a metal-

based biological strategy for hard flexible coatings. *Science* **328**, 216–20 (2010).

43. Roos, K. *et al.* OPLS3e: Extending Force Field Coverage for Drug-Like Small Molecules. *J. Chem. Theory Comput.* **15**, 1863–1874 (2019).

44. Gent, A. N. Adhesion and strength of viscoelastic solids. Is there a relationship between adhesion and bulk properties? *Langmuir* **12**, 4492–4495 (1996).

45. Yuk, H., Zhang, T., Lin, S., Parada, G. A. & Zhao, X. Tough bonding of hydrogels to diverse non-porous surfaces. *Nat. Mater.* **15**, 190–196 (2016).

46. Yuk, H. *et al.* Skin-inspired hydrogel–elastomer hybrids with robust interfaces and functional microstructures. *Nat. Commun.* **7**, 12028 (2016).

47. Desmond, K. W., Zacchia, N. A., Waite, J. H. & Valentine, M. T. Dynamics of mussel plaque detachment. *Soft Matter* **11**, 6832–6839 (2015).

48. Cohen, N., Waite, J. H., McMeeking, R. M. & Valentine, M. T. Force distribution and multiscale mechanics in the mussel byssus. *Philos. Trans. R. Soc. B Biol. Sci.* **374**, 20190202 (2019).

49. Motokawa, T. & Tsuchi, A. Dynamic Mechanical Properties of Body-Wall Dermis in Various Mechanical States and Their Implications for the Behavior of Sea Cucumbers. *Biol. Bull.* **205**, 261–275 (2003).

50. Sofla, A. Y. N., Meguid, S. A., Tan, K. T. & Yeo, W. K. Shape morphing of aircraft wing: Status and challenges. *Mater. Des.* **31**, 1284–1292 (2010).

51. Manti, M., Cacucciolo, V. & Cianchetti, M. Stiffening in soft robotics: A review of the state of the art. *IEEE Robot. Autom. Mag.* **23**, 93–106 (2016).

52. Montero De Espinosa, L., Meesorn, W., Moatsou, D. & Weder, C. Bioinspired Polymer Systems with

Stimuli-Responsive Mechanical Properties. *Chem. Rev.* **117**, 12851–12892 (2017).

53.   Capadona, J. R., Shanmuganathan, K., Tyler, D. J., Rowan, S. J. & Weder, C. Stimuli-responsive polymer nanocomposites inspired by the sea cucumber dermis. *Science* **319**, 1370–1374 (2008).

54.   Jorfi, M., Roberts, M. N., Foster, E. J. & Weder, C. Physiologically responsive, mechanically adaptive bio-nanocomposites for biomedical applications. *ACS Appl. Mater. Interfaces* **5**, 1517–1526 (2013).

55.   Balasubramanian, A., Morhard, R. & Bettinger, C. J. Shape-memory microfluidics. *Adv. Funct. Mater.* **23**, 4832–4839 (2013).

56.   Van Meerbeek, I. M. *et al.* Morphing Metal and Elastomer Bicontinuous Foams for Reversible Stiffness, Shape Memory, and Self-Healing Soft Machines. *Adv. Mater.* **28**, 2801–2806 (2016).

57.   Balasubramanian, A., Standish, M. & Bettinger, C. J. Microfluidic thermally activated materials for rapid control of macroscopic compliance. *Adv. Funct. Mater.* **24**, 4860–4866 (2014).

58.   Jin, H.-J. & Weissmüller, J. A material with electrically tunable strength and flow stress. *Science* **332**, 1179–1182 (2011).

59.   Overvelde, J. T. B. *et al.* A three-dimensional actuated origami-inspired transformable metamaterial with multiple degrees of freedom. *Nat. Commun.* **7**, 10929 (2016).

60.   Rocklin, D. Z., Zhou, S., Sun, K. & Mao, X. Transformable topological mechanical metamaterials. *Nat. Commun.* **8**, 1–9 (2017).

61.   Zhai, Z., Wang, Y. & Jiang, H. Origami-inspired, on-demand deployable and collapsible mechanical metamaterials with tunable stiffness. *Proc. Natl. Acad. Sci.* **115**, 2032–2037 (2018).

62.   Worrell, B. T. *et al.* Bistable and photoswitchable states of matter. *Nat. Commun.* **9**, 2804 (2018).

63.   Gu, Y. *et al.* Photoswitching topology in polymer networks with metal–organic cages as crosslinks.

Nature **560**, 65–69 (2018).

64.   Sosso, G. C. *et al.* Crystal Nucleation in Liquids: Open Questions and Future Challenges in Molecular Dynamics Simulations. *Chem. Rev.* **116**, 7078–7116 (2016).

65.   Rogerson, M. A. & Cardoso, S. S. S. Solidification in heat packs: I. Nucleation rate. *AIChE J.* **49**, 505–515 (2003).

66.   Rogerson, M. A. & Cardoso, S. S. S. Solidification in heat packs: II. Role of cavitation. *AIChE J.* **49**, 516–521 (2003).

67.   Rogerson, M. A. & Cardoso, S. S. S. Solidification in heat packs: III. Metallic trigger. *AIChE J.* **49**, 522–529 (2003).

68.   Wei, L. & Ohsasa, K. Supercooling and Solidification Behavior of Phase Change Material. *ISIJ Int.* **50**, 1265–1269 (2010).

69.   Dannemand, M., Schultz, J. M., Johansen, J. B. & Furbo, S. Long term thermal energy storage with stable supercooled sodium acetate trihydrate. *Appl. Therm. Eng.* **91**, 671–678 (2015).

70.   Guo, Q., Zaïri, F. & Guo, X. Thermodynamics and mechanics of stretch-induced crystallization in rubbers. *Phys. Rev. E* **97**, 052501 (2018).

71.   Cheng, N. G., Gopinath, A., Wang, L., Iagnemma, K. & Hosoi, A. E. Thermally tunable, self-healing composites for soft robotic applications. *Macromol. Mater. Eng.* **299**, 1279–1284 (2014).

72.   Shan, W., Lu, T. & Majidi, C. Soft-matter composites with electrically tunable elastic rigidity. *Smart Mater. Struct.* **22**, 085005 (2013).

73.   Schubert, B. E. & Floreano, D. Variable stiffness material based on rigid low-melting-point-alloy microstructures embedded in soft poly(dimethylsiloxane) (PDMS). *RSC Adv.* **3**, 24671–24679

(2013).

74.   Markvicka, E. J., Bartlett, M. D., Huang, X. & Majidi, C. An autonomously electrically self-healing liquid metal–elastomer composite for robust soft-matter robotics and electronics. *Nat. Mater.* **17**, 618–624 (2018).

75.   Park, J. *et al.* Three-dimensional nanonetworks for giant stretchability in dielectrics and conductors. *Nat. Commun.* **3**, 916–918 (2012).

76.   Hansen, C. M. *Hansen Solubility Parameters: A User's Handbook, Second Edition*. (CRC Press, 2007).

77.   Majidi, C. & Wood, R. J. Tunable elastic stiffness with microconfined magnetorheological domains at low magnetic field. *Appl. Phys. Lett.* **97**, 164104 (2010).

78.   Cao, C. & Zhao, X. Tunable stiffness of electrorheological elastomers by designing mesostructures. *Appl. Phys. Lett.* **103**, 041901 (2013).

79.   Narang, Y. S., Vlassak, J. J. & Howe, R. D. Mechanically Versatile Soft Machines through Laminar Jamming. *Adv. Funct. Mater.* **28**, 1707136 (2018).

80.   Brown, E. *et al.* Universal robotic gripper based on the jamming of granular material. *Proc. Natl. Acad. Sci.* **107**, 18809–18814 (2010).

81.   Maghooa, F., Stilli, A., Noh, Y., Althoefer, K. & Wurdemann, H. A. Tendon and pressure actuation for a bio-inspired manipulator based on an antagonistic principle. in *2015 IEEE International Conference on Robotics and Automation (ICRA)* 2556–2561 (IEEE, 2015). doi:10.1109/ICRA.2015.7139542.

82.   Stilli, A., Wurdemann, H. A. & Althoefer, K. Shrinkable, stiffness-controllable soft manipulator based on a bio-inspired antagonistic actuation principle. in *2014 IEEE/RSJ International Conference*

on Intelligent Robots and Systems 2476–2481 (IEEE, 2014). doi:10.1109/IROS.2014.6942899.

83. Amsden, B. Solute Diffusion within Hydrogels. Mechanisms and Models. *Macromolecules* **31**, 8382–8395 (1998).

84. Ogston, A. G., Preston, B. N. & Wells, J. D. On the Transport of Compact Particles Through Solutions of Chain-Polymers. *Proc. R. Soc. A Math. Phys. Eng. Sci.* **333**, 297–316 (1973).

85. Lorber, B. *et al.* Crystal growth of proteins, nucleic acids, and viruses in gels. *Prog. Biophys. Mol. Biol.* **101**, 13–25 (2009).

86. Qu, X., Wirsén, A. & Albertsson, A.-C. Novel pH-sensitive chitosan hydrogels: swelling behavior and states of water. *Polymer (Guildf).* **41**, 4589–4598 (2000).

87. Sumbre, G., Fiorito, G., Flash, T. & Hochner, B. Octopuses Use a Human-like Strategy to Control Precise Point-to-Point Arm Movements. *Curr. Biol.* **16**, 767–772 (2006).

88. Seppälä, A., Meriläinen, A., Wikström, L. & Kauranen, P. The effect of additives on the speed of the crystallization front of xylitol with various degrees of supercooling. *Exp. Therm. Fluid Sci.* **34**, 523–527 (2010).

89. Anseth, K. S., Bowman, C. N. & Brannon-Peppas, L. Mechanical properties of hydrogels and their experimental determination. *Biomaterials* **17**, 1647–1657 (1996).

90. Flory, P. J. *Principles of Polymer Chemistry*. (Cornell University Press, 1953).

91. Liu, Y. Determination of Flory interaction parameters between polyimide and organic solvents by HSP theory and IGC. *Polym. Bull.* **509**, 501–509 (2008).

92. Hertz, H. Hertz's miscellaneous papers. *McMillan, London* **55**, 6–9 (1896).

List of publications

Yang, F., Cholewinski, A., Yu, L., Rivers, G. & Zhao, B. A hybrid material that reversibly switches between two stable solid states. *Nat. Mater.* **18**, 874–882 (2019).

Yang, F., Cholewinski, A. & Zhao, B. Algae–mussel-inspired hydrogel composite glue for underwater bonding. *Mater. Horizons* **6**, 285–293 (2019).

Cholewinski, A., **Yang, F. K.** & Zhao, B. Glycerol-Stabilized Algae-Mussel-Inspired Adhesives for Underwater Bonding. Ind. Eng. Chem. Res. (2020) doi:10.1021/acs.iecr.0c02531.

Zhang, W., Wang, R., Sun, Z. M., Zhu, X., Zhao, Q., Zhang, T., Cholewinski, A., **Yang, F.**, Zhao, B., Pinnaratip, R., Forooshani, P. K. & Lee, B. P. Catechol-functionalized hydrogels: biomimetic design, adhesion mechanism, and biomedical applications. *Chem. Soc. Rev.* **49**, 433–464 (2020).

Cholewinski, A., **Yang, F. K.** & Zhao, B. Underwater Contact Behavior of Alginate and Catechol-Conjugated Alginate Hydrogel Beads. *Langmuir* **33**, 8353–8361 (2017).